ABSTRACT

Title of Thesis:	The Structure of the Blue Whirl: A Soot-Free Reacting Vortex Phenomenon
	Sriram Bharath Hariharan Master of Science 2017
Thesis Directed By:	Michael J. Gollner Assistant Professor Department of Fire Protection Engineering

Recent experiments have led to the discovery of the blue whirl, a small, stable flame that evolves from a fire whirl, and burns typically sooty hydrocarbons without producing soot. The distinct physical structure of the flame is investigated through digital imaging techniques, which suggest that the transition and shape of the flame may be influenced by vortex breakdown. The thermal structure of the blue whirl reveals a peak temperature around 2000 K, and that most of the combustion occurs in a relatively small, visibly bright vortex ring. The formation of the flame is shown to occur over a variety of surfaces, including water and flat metal, all of which indicate that the formation of the blue whirl is strongly influenced by the flow structure over the incoming boundary layer. Finally, a schematic structure of the blue whirl is proposed, based on the measurements presented here and previous literature on fire whirls and vortex breakdown.

THE STRUCTURE OF THE BLUE WHIRL: A SOOT-FREE REACTING VORTEX PHENOMENON

by

Sriram Bharath Hariharan

Thesis submitted to the Faculty of the Graduate School of the
University of Maryland, College Park, in partial fulfilment
of the requirements for the degree of
Master of Science
2017

Advisory Committee:

Professor Michael J. Gollner, Chair
Professor Elaine S. Oran, Co-advisor
Professor Peter B. Sunderland

Acknowledgements

Words cannot begin to explain my gratitude to Dr. Michael J. Gollner, who has truly been an inspiration, guide and friend over the past two years. My heartfelt thanks to Dr. Elaine S. Oran, a mentor who has been influential in motivating my inquisitive attitude. I am indebted to them for giving me the opportunity to work on this project, for constantly believing in me, and encouraging me to showcase my best.

My sincere thanks to Dr. Peter B. Sunderland for being on my advisory committee, and more importantly, facilitating my acceptance to the graduate program at UMD. I thank him and Paul M. Anderson for allowing me to borrow the UV camera for experiments. Paul, thank you for never hesitating to answer my endless list of questions.

This work was supported by the National Science Foundation through awards CBET – 1507623 and 1554026, and by the University of Maryland through the Minta Martin Endowment Funds in the Department of Aerospace Engineering and the Glenn L. Martin Institute Chaired Professorship at the A. James Clark School of Engineering.

Thank you to Hugh Spilker at Orbital ATK (COI Ceramics, Inc.) for providing the SiC fibre samples used in this study.

Huahua Xiao, Evan Sluder, Erin Griffith, Ali Tohidi and Yu Hu have been extremely helpful in assisting me with experiments and analysing data. I thank Ajay Singh for promptly addressing my questions over email.

Thank you to Lin Jiang for patiently teaching me to assemble thermocouples, and Nate May for ensuring safety in the lab when experiments didn’t go as planned. I

thank everyone in the lab group, and all my colleagues in the Department of Fire Protection Engineering for always being ready to lend a hand.

Special thanks to Mary Lou Holt and Sharon Ann Hodgson for making paperwork a breeze, and other department staff who have always been helpful.

I thank Alok Mukundan for aiding my initial efforts in learning to use a camera, which has been pivotal in presenting this work. The wonderful pictures of the blue whirl are testament to his help.

The Department of Mechanical Engineering has been gracious in supporting me as a TA over the past three semesters.

I thank Dr. Rammohan Y. S., Dr. Mallikharjuna Babu and Dr. Rathanraj K J from BMS College of Engineering, Bangalore for encouraging me to pursue my graduate studies.

Finally, I express my gratitude to my family for their constant support and reassuring encouragement.

Table of Contents

List of Tables

List of Figures

Terminology

TFP	Thin-Filament Pyrometry
HFR	High Frame Rate
Γ	circulation
Ω	swirl number
ν	kinematic viscosity
T_g	gas temperature
T_{tc}	thermocouple temperature
T_{surr}	ambient temperature
ε_{tc}	emissivity of thermocouple bead
d_w	wire diameter
U	fluid velocity
k	thermal conductivity
σ	Stefan-Boltzmann constant

Chapter 1: Introduction

Fire whirls have been studied in fire science literature because of the dangers they present during large urban and wildland fires [1–3]. While buoyant gases ordinarily move upward in a convection column or plume over a burning area, fire whirls result in more violent and organized convection currents resulting in a tall, slender vortex of yellow flames [2]. While investigating the formation of such fire whirls in a fixed-frame self-entraining apparatus to study oil spill remediation over a water surface, a new regime of the fire whirl, the blue whirl" was recently discovered [4]. The blue whirl appeared as an inverted blue cone hovering directly over the water surface. At the edge of the blue cone was a bright rim that burned without any traces of yellow, indicating soot free combustion, even when directly burning ordinarily sooty liquid fuels. Above the blue cone and bright rim, a purple haze was seen.

The yellow colour in a flame originates from black body radiation of soot particles, similar to that observed in a candle flame. An instane of a sooting flame is visible in *Figure 1a*, showing a fire whirl generated in a suction type fire whirl setup. In contrast, a blue whirl shows very few signs of the presence of soot. In *Figure 1b*, a blue whirl formed using heptane over a water surface is shown. The considerable difference in physical structure to a traditional yellow fire whirl is apparent. In *Figure 1b* (captured with an exposure time of 12.5 ms), a yellow soot streak is seen exiting the flame through the purple haze region, showing the fleeting nature of soot within the blue whirl. A yellow fire whirl generated in the same setup within which the blue whirl was observed (with ~10 ml n-heptane), shown in *Figure 1c* is very luminous due to its

high soot content, similar to *Figure 1a*. Fire whirls similar to the one in *Figure 1c* evolved into the small blue whirl without any mechanical eddy-generation mechanisms such as blowing, suction, or rotating meshes which have previously been used to study fire whirls. Discovery of this flame regime is surprising, given the considerable literature that has studied fire whirls over the past few decades. With concerns of global climate change increasing, a combustion or remediation solution that offers reduced pollution levels, with relatively simple mechanical complexity, ultimately offers more flexibility in design of machines that depend on combustion to convert energy. The blue whirl, due to its low-sooting nature and natural formation, has the potential to offer such benefits, and consequently motivates a deeper understanding of the governing processes, to aid in developing engineering solutions in the future.

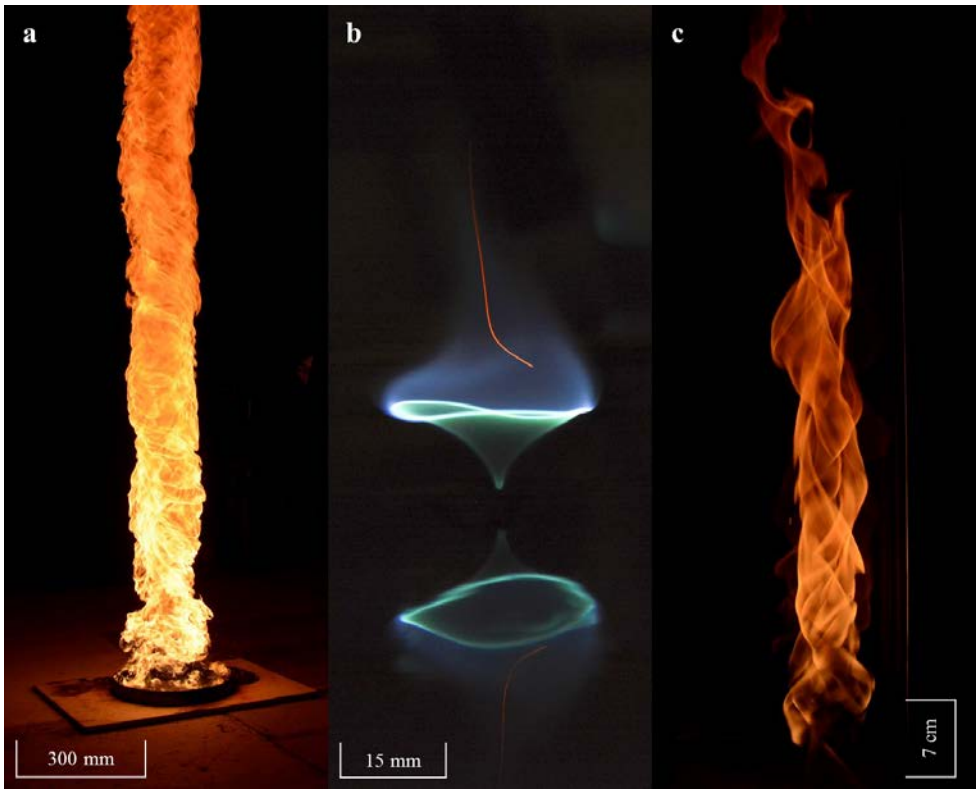

Figure 1. Images of (a) yellow fire whirl in a suction-type setup, (b) the blue whirl (reflection below), and (c) yellow fire whirl prior to blue whirl formation.

Since the flame appears directly over a pool of liquid fuel, the blue whirl may offer some interesting solutions to a variety of engineering challenges. As Lin and Faeth described, “soot-free hydrocarbon fuelled diffusion flames are of significant interest because many practical combustion processes achieve this condition to avoid soot emissions” [5]. The phenomenon is quite fascinating as no external forcing was employed. The flame was observed to evolve of its own accord to assume this beautiful shape, whereas previous studies relied on specific flow configurations of gaseous fuel and oxidizer that were required to observe blue flames [5,6].

The occurrence of the phenomenon raises many questions. The physical structure, nature of combustion, resulting thermal structure, and fluid flow field are important pieces of the puzzle. How these differ from a traditional fire whirl is also an important question in addressing its delayed discovery. Defining the conditions required to observe the phenomenon are also of interest, including explaining why the blue whirl has not been seen before, despite evolving from a traditional fire whirl that has been under intensive study for decades. The objectives of this work are therefore, to understand the structure and formation of the blue whirl, attempting to answer some of these questions. Fundamental explanations of the processes governing its formation and structure are proposed based on the results obtained through the use of digital imaging, micro-thermocouples, thin-filament pyrometry, and OH* spectroscopy, which together provide detailed insight into the physical mechanisms influencing the formation, and structure of the blue whirl.

Chapter 2: Literature Review

2.1 The Fire Whirl

This section provides a short background on existing fire whirl literature. Essential information deemed relevant for making comparisons with the blue whirl are presented here, but a more detailed review on efforts to understand fire whirls is presented in [7].

2.1.1 Formation and Conditions

Fire whirls are known to form under combinations of wind and fire that result in whirling flames with a significant intensification of combustion [7]. The three essential conditions governing the formation of the fire whirl, as defined by Byram and Martin [2] are:

i. The presence of an eddy, and an eddy generating mechanism
ii. A fluid sink present within the eddy
iii. Friction or drag to the air movement at the lower boundary by a horizontal surface

In the laboratory, the eddy/vortex may be generated using a number of different apparatus – a rotating mesh [3], tangential slits in an enclosure [2,8,9], or multiple air curtains [10] to sustain the fire whirl. The convection column resulting from a fire whirl acts as the fluid sink, and the surface over which the fire whirl occurs provides the friction or drag. Schematics of common configurations used to generate fire whirls in a laboratory are shown in *Figure 2*. Circular intake configurations may sometimes be

supplemented with a suction at the outlet. The fire whirl in *Figure 1a* was generated using configuration *2b* along with a suction mechanism. When liquid fuels are used, a metal pan is used to contain fuel at the base in all configurations [3,11–13]. Alternately, a gas burner may be used at the base of an enclosure [9,14–17]. Outside of the laboratory, wind, obstacles, and interacting fires [18] are known to produce fire whirls during large wildland or urban fires [19]. In all of these cases, it appears that a critical balance between buoyancy, produced as a result of the heat release, and circulation, induced by surrounding obstacles and wind, are required to generate an initial vortex that results in the traditional yellow fire whirl [15,16]. Recent studies [20] have shown several regimes that can occur before the transition of a pool fire into a fire whirl, providing a detailed classification of the different forms assumed by a traditional yellow fire whirl under various combinations of circulations and heat release rates [16].

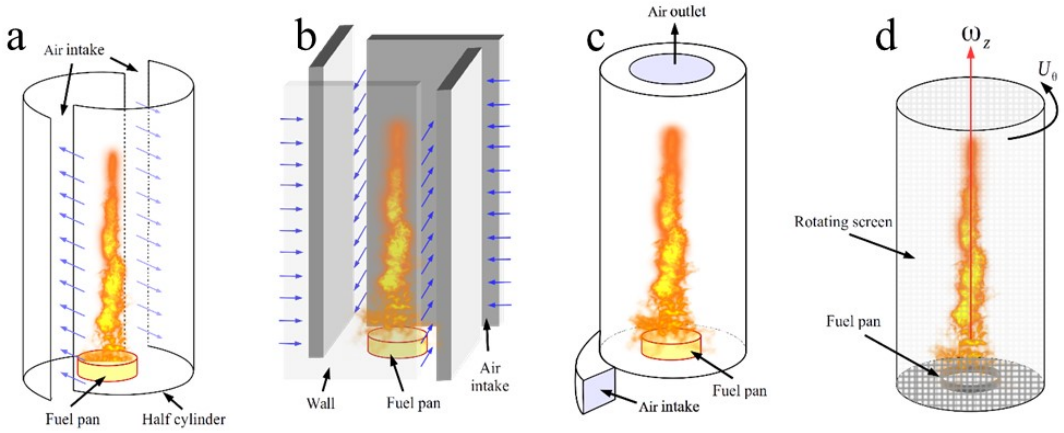

Figure 2. Configurations used to generate fire whirls in a laboratory, from [7]. (a) half-cylinders with slits, (b) walls with slits, (c) circular intake, (d) rotating mesh setup.

2.1.2 Structure of the Fire Whirl

Emmons and Ying [3] presented detailed measurements of a fire whirl generated using a rotating mesh setup. A fuel dish was placed on the floor at the centre of the enclosure and continuously replenished with acetone. Flame wander was observed, i.e. the flame was observed to move in a circular pattern around the enclosure, and hence measurements obtained in the study were adjusted through visual observations. The temperature distribution (shown in *Figure 3*) was obtained using a tungsten resistance thermometer across the fire whirl at various circulation strengths. Similar results were obtained by Lei et al. [17] using K-type thermocouples. These results led to the conclusion that the core of the fire whirl was fuel-rich, with most reaction occurring as a diffusion flame close to the edge of the vortex core. Further, it was shown that the burning rate increased monotonically with ambient circulation. It was also proposed that surface waves could exist at the surface of the core, if vortex breakdown were to occur. Similarities and differences of these results with those of the blue whirl are discussed in section *5.2*.

The rotating mesh setup of Emmons and Ying [3] was observed to produce a free vortex within the enclosure, with a circulation equal to ~87% of the mesh. This, and other investigations have led to the approximation of the vortex core as a rigid body surrounded by a free vortex. This was confirmed by recent stereo PIV measurements [9,14]. The Rankine vortex model [2,8], and the Burgers vortex model [13,17,21,22] have been used to define the vorticity field in a fire whirl. Tohidi et al. [7] conclude that although some studies [23,24] have reported that the Burgers vortex model does not adequately describe the radial distribution of azimuthal velocity, existing

experimental data fits best with this model for a quasi-steady on-source fire whirl [9,14,17].

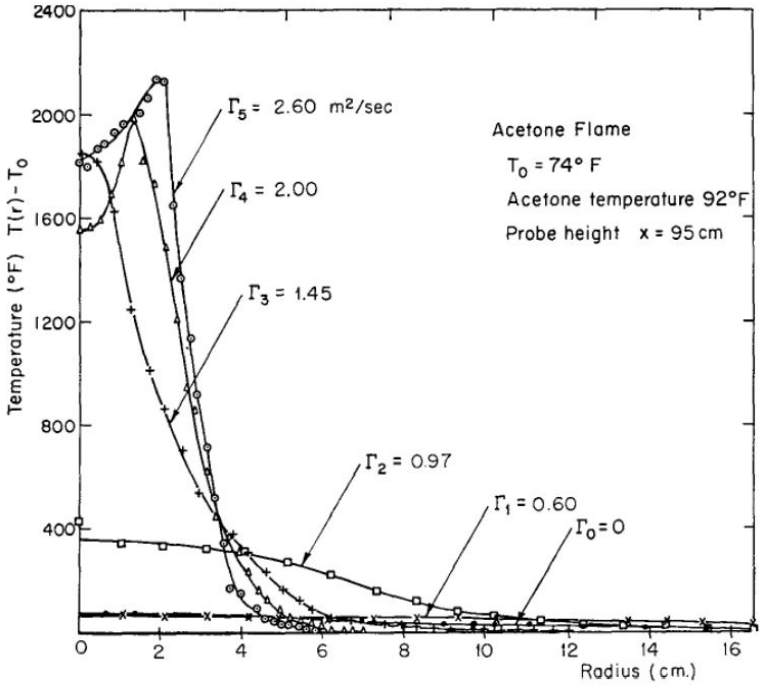

Figure 3. Radial distribution of mean temperatures in a fire whirl as reported by [3].

A detailed study of the velocity field of a fire whirl was performed in [14]. The results are reproduced in *Figures 4 and 5*. A fixed-frame, self-entraining setup was used with an ethanol pool as the fuel. Stereo-PIV was used to measure the azimuthal and axial velocities in the fire whirl. Measurements were recorded for different conditions, first by varying the height at which measurements were taken for a given slit width in the setup, and then by varying the slit widths for a given height. *Figure 4* shows that azimuthal velocity measurements adhere to the Burgers vortex model, which has a smoother transition to the free vortex region outside the vortex core than the Rankine vortex model. Also depicted is the radial distribution of circulation, which at the edge of the vortex core was found to be ~0.7 times the ambient circulation.

Similarly, the axial velocity profiles depicted in *Figure 5* show the effect of buoyancy generated by the combustion in the fire whirl.

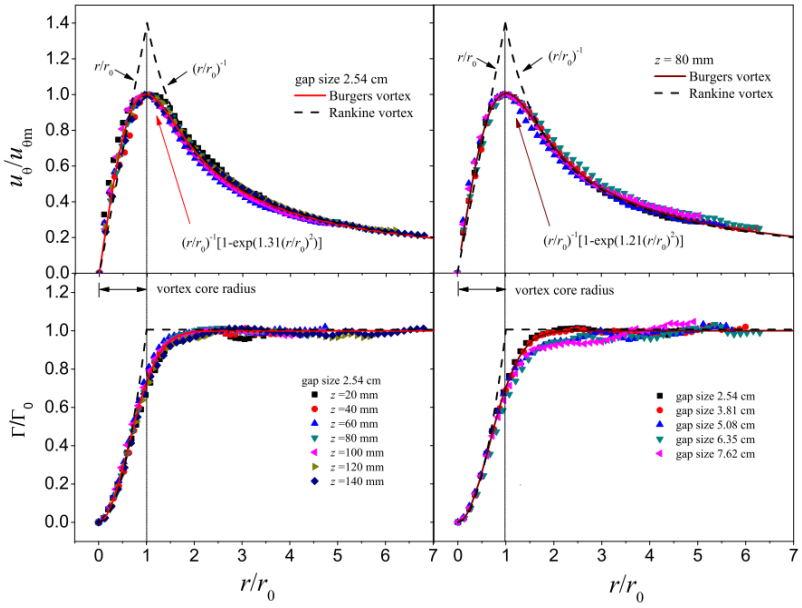

Figure 4. Normalized plots of azimuthal velocity and circulation with radius in a fire whirl as reported in [14]. Left - Measurements at different heights for a given slit width. Right - Measurements at a given height for different slit widths.

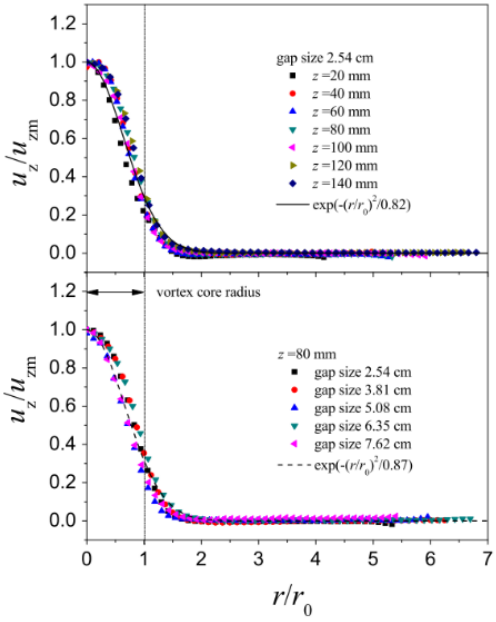

Figure 5. Normalized plots of axial velocity with radius in a fire whirl as reported in [14]. Top - Measurements at different heights for a given slit width. Bottom - Measurements at a given height for different slit widths.

2.1.3 The blue whirl

The blue whirl may be classified as a small scale, on-source whirl [7]. At the time of Xiao et al.'s first publication [4], little was known about the structure of the flame or the conditions required for its formation. The flame was discovered while evaluating possibilities of efficient oil spill remediation using fire whirls, and proposed that the regime could be used for fluid mechanics research, particularly that of vortex breakdown in reacting flows. The blue whirl state could be sustained in the laboratory as long as fuel supply was maintained, indicating that the occurrence of the phenomenon was not a brief transition, but a stable regime in itself. The smooth boundary of the water surface was thought to contribute to the formation of the blue whirl structure. Although initial discovery of the blue whirl was made over a water surface, it will be shown in this study that the water surface is not indispensable for the blue whirl to form, but the surface over which the whirl forms must be continuous and unimpeded without the presence of any vertical protrusions.

It was also proposed by Xiao et al. [4] that fast mixing and the swirl in the enclosure provided the right conditions to reduce or eliminate soot formation, based on previous observations in strained diffusion flames [25,26]. In addition to the blue whirl, a transitional-blue whirl, observed as a blue cup holding a yellow flame was also reported. It was suggested that the low-sooting nature of the flame was due to the increased residence times of premixed reactants within the recirculation zones of the reactive vortex breakdown bubble, and that a general triple flame structure may be expected.

In general, due to its small size, the blue whirl was expected to be a laminar flame based on visual observations, similar to prior findings on lower sections of a fire whirl [11]. The temperature distribution presented here reveals that the temperature varies with axial position. As a result, the level of circulation and axial velocity may also vary with axial position in the different regions of the flame, since within a fire whirl core, vorticity, temperature, and axial velocity are all coupled [7,17].

2.2 Vortex Breakdown

Vortical flows have wide applicability in engineering systems. They have been used in combustion systems (typically utilizing diffusion flames) to achieve control over the rate of mixing between fuel and air, such that an appropriate heat release could be produced [27]. According to Leibovich [28], vortex breakdown is a disturbance created by a characteristic ratio of tangential to axial velocity, leading to the formation of a stagnation point and recirculation zone on the vortex axis. The formation of the stagnation point is promoted by the presence of an adverse pressure gradient. Vortex breakdown is typically observed when the tangential speed at the edge of the vortex core is more than the axial speed within the core. Various flow patterns can result from this disturbance, and the specific pattern that evolves depends upon the swirl (which controls the tangential velocity) and Reynolds number (which controls the axial velocity). The most common breakdown patterns observed are the "bubble" (*Figure 6*) and "spiral" (*Figure 7*) modes of vortex breakdown. The structure of these breakdown regions may be divided into three zones [28]:

i. The approach region which consists of the vortex core, with axial speeds in the core in the range of the maximum azimuthal speeds.

ii. The breakdown region, occupying an axial interval approximately 5 times the vortex core diameter. The region may further be divided into three sub-divisions, the third of which is characterized by transition to turbulence.

iii. A downstream vortex, possessing an expanded core, and minimal axial variations.

Visual observation of flow around a vortex breakdown "bubble" (performed in [29]) is similar to that of a solid body in the path of a fluid, resulting in a wake downstream, where conditions similar to the upstream may be restored. In the region of breakdown, a strong coupling between the azimuthal (tangential) and axial velocities exists, and the recirculating motions within the "bubble" act as an aerodynamic three-dimensional bluff body, around which, according to Harvey [29], "the fluid is obliged to flow." According to Leibovich [28], vortex breakdown, which exhibits flow reversal in a limited axial interval, is a regime that is intermediate between weakly and rapidly swirling flows. In combusting systems, the occurrence of a vortex breakdown bubble serves as an aerodynamic blockage that stabilizes flames [30], and has been observed prior to lean-blowout of gas turbine combustors [31]. Further discussion of this phenomenon will be limited to experimental investigations, although several numerical simulations have been carried out in this regard [32,33]. Early experimental work on vortex breakdown was performed in non-reacting flows (cold-flow), typically using water and a coloured dye for flow visualization.

2.2.1 Classification of Vortex Breakdown

This section presents a brief discussion of three of the most commonly observed modes of vortex breakdown. Depending on the swirl and Reynolds numbers of water flowing in a cylindrical tube, seven types of vortex disturbances were identified, three of which are of the axisymmetric type (Types 0, 1, 2). In general, Type 0 and Type 2 forms are usually referred to as "axisymmetric" in literature, and hence, in this work as well. However, the vortical axis (also called swirl axis) of these disturbances do not strictly coincide with the geometrical axis of the apparatus used to conduct experimental investigations [34]. The different types were characterized experimentally using a liquid dye tracer in water [35–37].

Type 0: Bubble

This is an axisymmetric type of breakdown, containing a stagnation point on the vortex axis. The bubble is characterized by simultaneous filling and emptying [35] in one of two ways – first, at diametrically opposite ends in the azimuthal direction, at the upstream end of the bubble, or second, with filling taking place at an upstream point and emptying taking place at a downstream point, such that the tail returned to the vortex axis, resulting in a second disturbance one bubble length downstream of the first breakdown. The second disturbance was typically found to be of Type 2, namely a spiral mode.

Type 2: Spiral

At specific combinations of Reynolds number and swirl, the dye filament (in the vortex axis) used in the experiments was found to end abruptly in a stagnation point,

form a kink and then form a cork-screw shape [37]. The filament was observed to break up into turbulence afterwards.

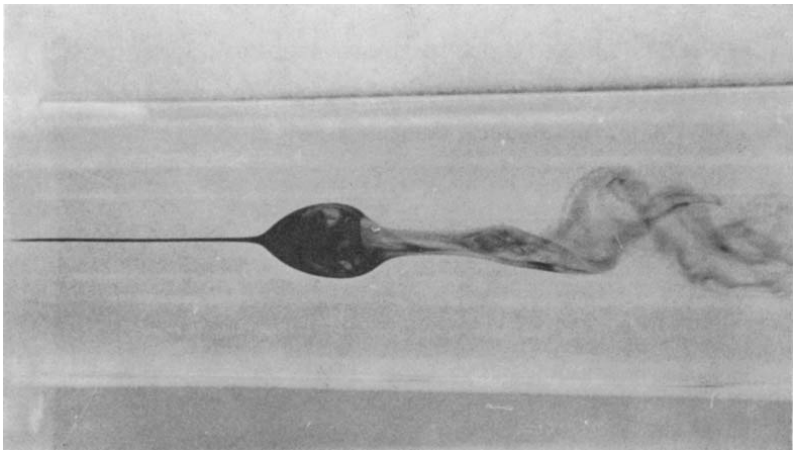

Figure 6. Image of a vortex breakdown bubble (Type 0) from [38].

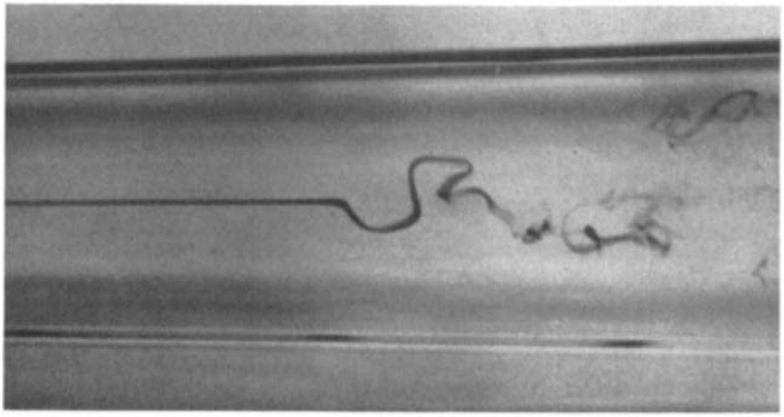

Figure 7. Image of an instance of spiral vortex breakdown (Type 2) from [28].

Type 5: Double-helix

At low Reynolds numbers, two different helical paths of dye emanated from the kink (*Figure 8*). The filaments were usually observed to shear and form tapes that followed the same rotation of the base flow. Dye filaments, injected off-axis resulted in distortion upstream of where the central filament experienced disturbances, resulting in forms that were “indescribably complex” [37]. These helical filaments were

observed to noticeably expand and eventually reach the walls of the pipe that was used to conduct experiments. According to [36], the double helical mode is just an extension of the tape-like Type 6 breakdown, but has been classified as a separate type due previous reports of the structure in [35]. The Type 5 disturbance was observed to form directly from the Type 6 disturbance. Further detailed discussions are provided in [37] and [36].

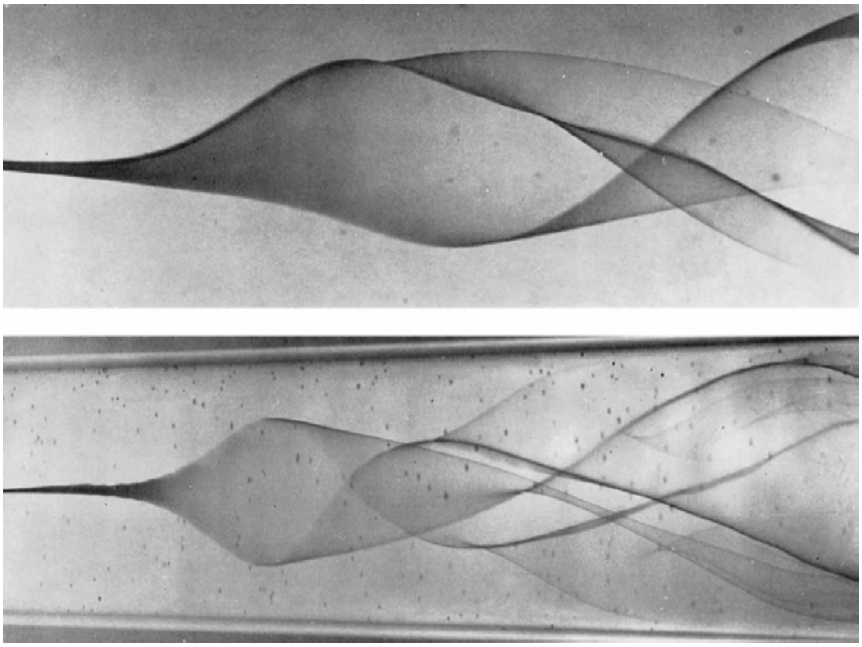

Figure 8. Images of the double-helix (Type 5) vortex breakdown from [35].

2.2.2 Envelope of occurrence

A map of the different flow conditions resulting in the various vortex disturbance forms was compiled by Faler and Leibovich [37] and is depicted in *Figure 9*. In general, for a given flow rate, a higher circulation was more likely to generate the Type 0 disturbance, as compared to the levels required to generate the Type 2 disturbance. Similarly, for a given circulation, a higher flow rate resulted in the

recirculating bubble mode (Type 0). The mean axial location varies based on a combination of the flow rate, circulation and the type of the resulting disturbance. The axial position is determined by the position of the nose (or downstream end) of the bubble. The occurrence of Types 3-6 is limited to low Reynolds numbers [36]. Here, the Reynolds and circulation numbers are defined as $Re=U_0D_0/\nu$, and $\Omega = \Gamma/U_0D_0$, respectively.

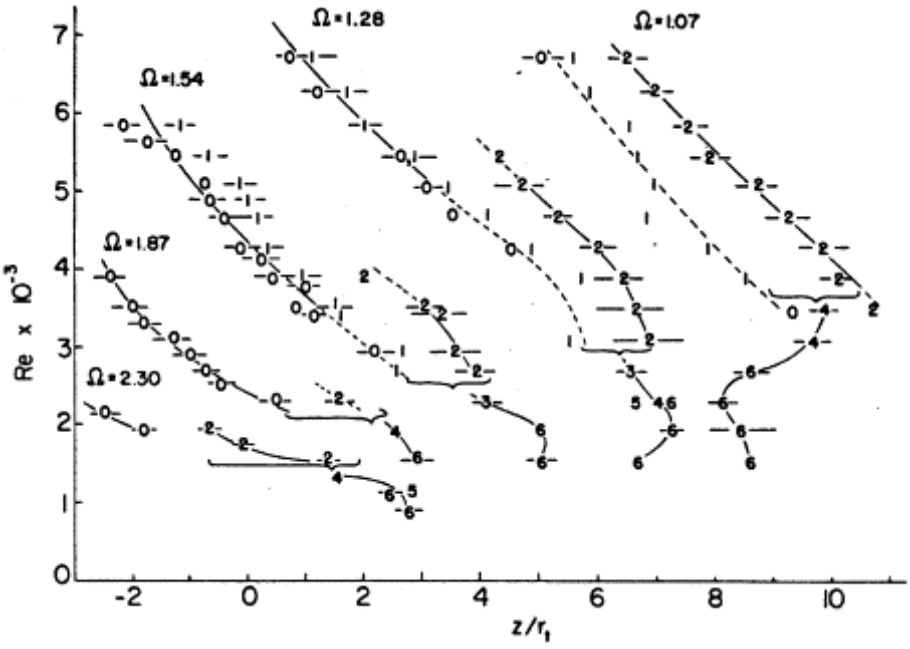

Figure 9. A map of the different types of vortex disturbances formed. The axial positions are plotted against the Reynolds number of flow for varying levels of circulation at the pipe inlet [37].

In *Figure 10* (from [35]), the circles denote the axisymmetric breakdown bubble, and the triangles represent the spiral mode. Open markers correspond to experimental conditions with fixed vane angles (and hence, circulation number), while filled markers correspond to fixed flow rate conditions. The slight differences in the different experimental conditions are discussed in [36]. Also, the dependence of the

occurrence of the various forms of disturbances on Reynolds number need to be regarded as the effect of vorticity, and not viscosity [27].

Since it was suggested that the blue whirl may be a reactive bubble mode regime [4], a "map" similar to ***Figure 9*** is expected to exist for the blue whirl. A map similar to ***Figure 10*** (from [35]) is more appropriate as it depicts only the bubble and spiral modes. Differences in the blue whirl map could stem from buoyancy resulting from combustion.

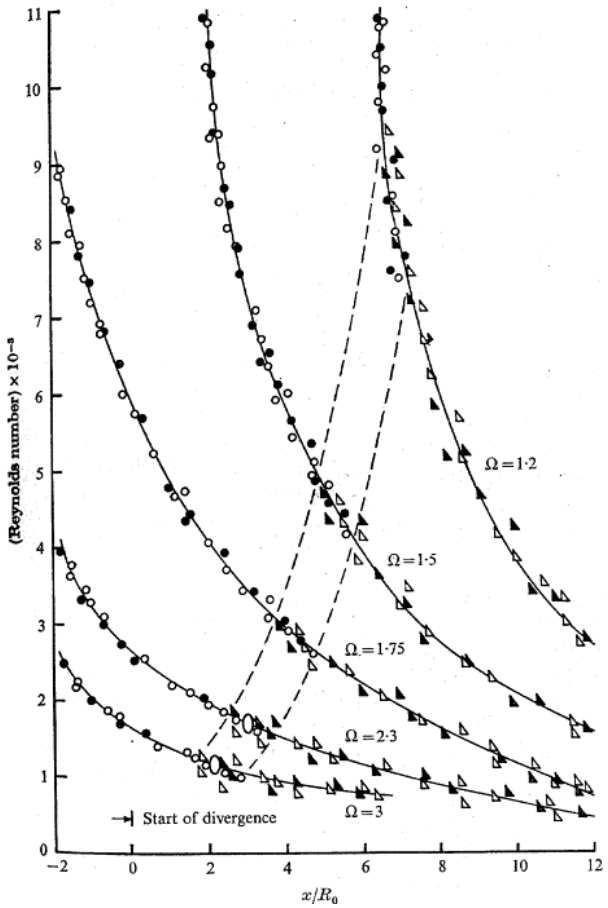

Figure 10. A map compiled by Sarpkaya [35], showing the axial position of the spiral and bubble modes of vortex breakdown plotted against Reynolds number for different levels of circulation.

2.2.3 Velocity Profiles and Recirculation Zones

In addition to mapping the variation of the spatial location of the breakdown with Reynolds and circulation numbers, Faler and Leibovich [38] investigated the internal structure of the axisymmetric vortex breakdown bubble by developing detailed velocity profiles (*Figure 11*) using laser Doppler anemometry. The results yielded fluid streamlines (*Figure 12*) revealing fluid recirculation zones, and four stagnation points on the axis. Other studies [34][37] utilizing Particle Tracking Velocimetry and laser scanning reaffirmed previous observations in [35] that bubble filling occurred at the downstream end, and emptying occurred at the upstream end of the vortex ring. Based on these measurements, similarities were observed between the bubble and spiral forms [34], and it was suggested that the bubble mode was just a 'compressed' spiral [27]; the observed form depended on the slope, extent of winding and the diameter of the vortex core.

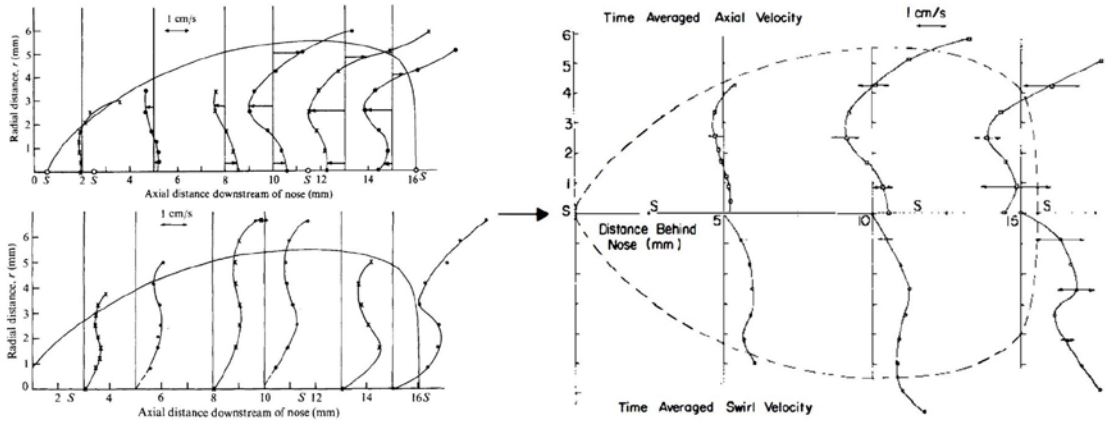

Figure 11. Axial (top-left) and swirl (bottom-left) velocity profiles as measured in [38]. A reduced representation of both velocity components (right), from [28].

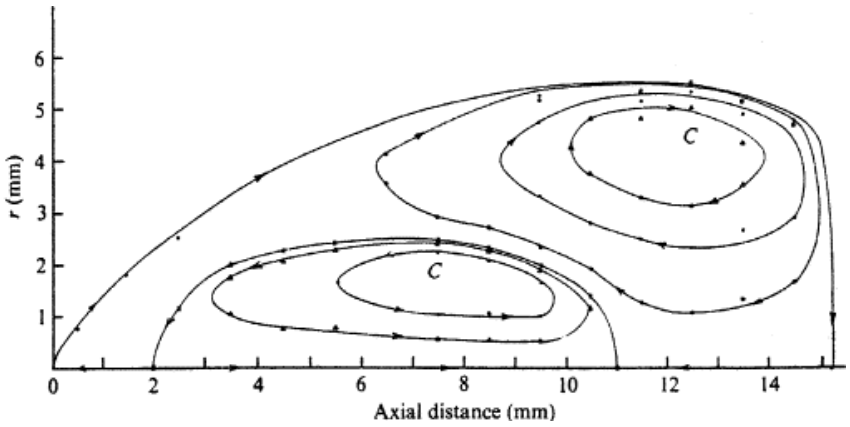

Figure 12. Streamlines within the bubble derived from velocity measurements [38].

2.3 Other concepts

Non-sooting flames with reduced NO_x emissions have been reported before [6]. The turbine combustor designed in [40] based on the asymmetric whirl combustion concept involved asymmetric injection of gaseous fuel (methane) into a high swirl combustor. The forced, strong swirl combustor burning a gaseous fuel under overall lean conditions (Φ < 0.38) produced a blue flame under asymmetric fuel injection, while a whirling yellow flame was observed under symmetric injection. Another study [31] found that both bubble and spiral-type vortex breakdowns were observed near lean blowout, and suggested that it could be used as flame stabilizers in atmospheric conditions.

In contrast to these configurations, the blue whirl involves direct burning of liquid fuels that are known to be sooty. In addition, forced flow is not employed, and the self-entraining flow is regulated only by the combustion-induced buoyancy within the enclosure. Considering the simplicity of the procedure employed in this study, it is surprising that the blue whirl regime has not been reported before. As yet, the type of

flame structure that best describes the blue whirl is unclear, but could be a triple flame [4], or even an edge flame [41].

Chapter 3: Experimental Methods

This chapter provides details on the experimental apparatus, procedures, and the methods of analysis employed in this study. First, a description of the general apparatus is presented, followed by specific details on thin-filament pyrometry and OH* spectroscopy.

3.1 Experimental Apparatus

A fixed-frame configuration is used in this study due to its mechanical simplicity. An enclosure was created with two half-cylinders (made of fused quartz) offset by a small distance to create rectangular slits at each end. This configuration allows for easy probing of the flame within the enclosure. Since air flow and vorticity are controlled solely by the buoyancy generated by the flame within the enclosure, this may be termed as a self-entraining configuration. Once the fuel is ignited, buoyant convection of gaseous products results in air surrounding the enclosure to entrain tangentially through the two slits, generating swirl within the enclosure. The two quartz half-cylinders were suspended on an aluminium frame assembled using T-slot erectors (80/20 Inc.). The frame permitted 2-dimensional positioning (vertical position and slit width) of the two quartz half-cylinders, and independent control of the two cylinders. This arrangement was placed over a water pan (40 cm diameter).

The slit width is expected to determine the entrainment velocity, and thus the swirl within the enclosure. A fire whirl may be formed within a wide range of slit widths. In this self-entraining configuration, a relatively narrower range of slit widths exists (in combination with a particular fuel supply rate), within which a fire whirl will

transform into a blue whirl. The direction of the vortex formed within the enclosure is determined by the slit orientation, and in this study, both clockwise and anticlockwise orientations were observed to produce similar results.

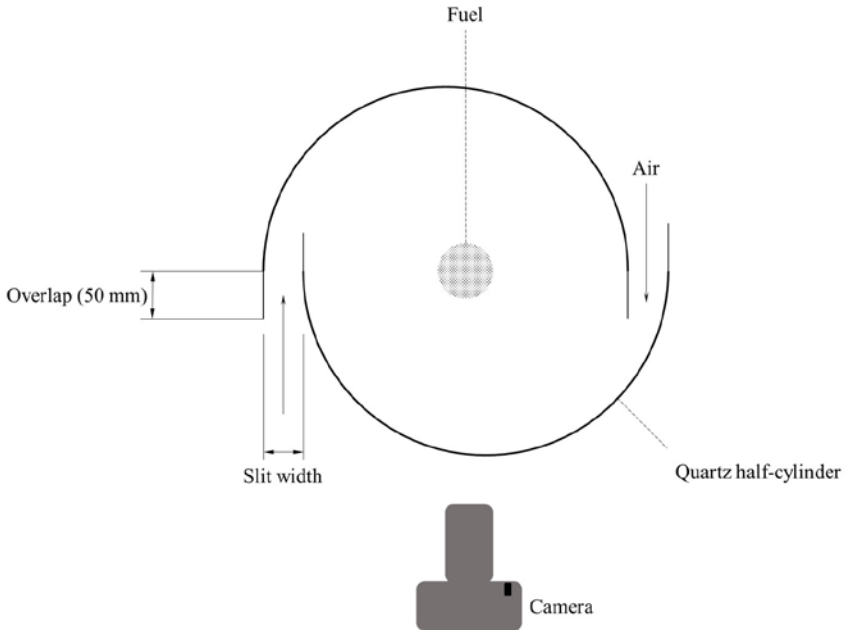

Figure 13. Top view of experimental setup.

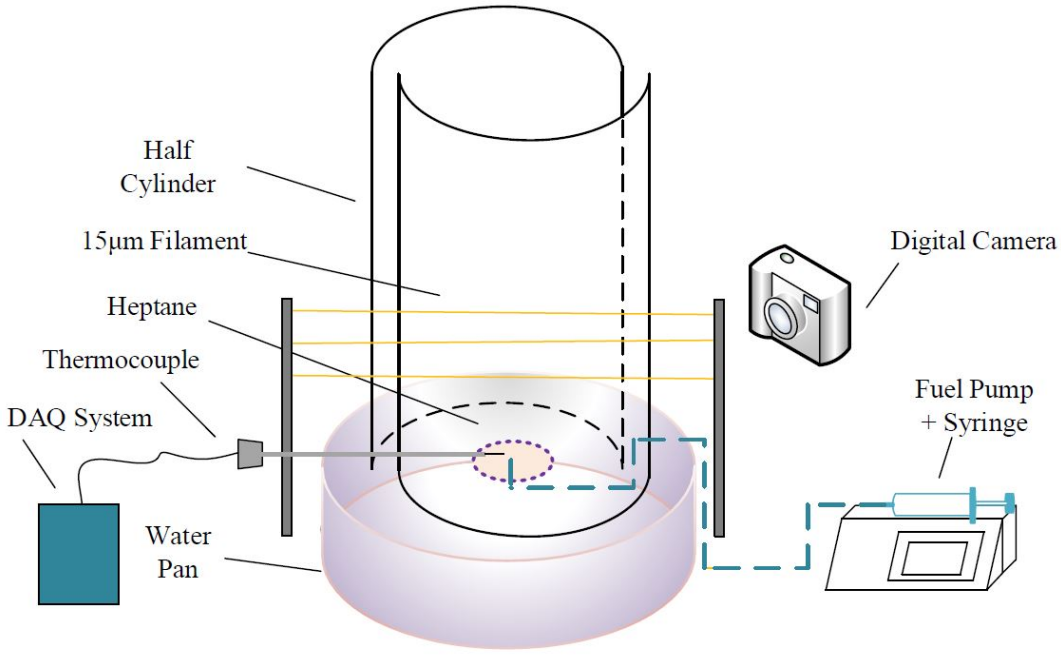

Figure 14. Detailed experimental setup.

Experiments were repeated with two different pan depths – 3.2 cm (made of stainless steel) and 12.2 cm (made of quartz). No discernible difference was observed in the development of the fire whirl or the blue whirl when either pans were used. Therefore, the smaller 3.2 cm deep pan was used for all tests reported here due to the smaller quantity of water required, which improved operability of the setup. The half-cylinders had a diameter of 32 cm and a height of 60 cm. The cylinders were positioned such that was no overlap when viewed in a radial direction in line with the two slits (*Figures 13 and 14*). A short overlap region (50 mm) was constructed separately using aluminium tape along each end. This permitted insertion of probes by removing the tape only at required locations. For thin-filament pyrometry (TFP), the aluminium tape was not present on either side up to a height of 11 cm above the water surface to allow the filaments to pass through across the centre of the enclosure.

Heptane (99.4% pure) temporarily stored in a syringe (Becton Dickinson 60 ml with a Luer-Lok^{TM} Tip), the primary fuel used in this study, was injected using a syringe pump (Harvard Apparatus Pump 11 Elite) through a copper tube (3 mm OD, 1.5 mm ID). A small piece of copper wire was projected out of the opening in the copper tube, such that the copper wire was just below the water surface to prevent the fuel from bubbling to the surface. The syringe diameter and required fuel pumping rate were programmed into the syringe pump system.

The positions and settings of cameras used for various diagnostics were selected based on the information desired from the obtained image. Relevant details, along with settings under which these instruments were operated, are provided in *Chapter 4: Results*.

With this configuration in place, a typical experiment involved the injection of fuel (~2.5 ml) onto the water surface, followed by ignition using a butane torch. Continuous supply mode in the syringe pump was turned on if sustained presence of either the fire whirl or blue whirl was required. Depending on the diagnostics employed, either the camera, or thermocouple data acquisition system was started, along with video capture, and synchronized at the beginning of the experiment.

3.2 Micro-Thermocouple Measurements

Micro-thermocouples were used to probe the temperature of the blue whirl. Due to the continuous precession of the blue whirl within the enclosure, and because a thermocouple provides a measurement at only a single spatial location at a given time, this technique is utilized to obtain a unidirectional temperature profile of the blue whirl along the axial direction (refer *Figure 43* in the *Appendix* for a schematic). R-type thermocouples (Pt/13%Rh-Pt) of two different sizes – 50 μm and 75 μm, were threaded into a two-hole ceramic tube (1.6 mm OD), with the bead projecting out of the ceramic tube approximately 5 mm. This probe (approximately 25 cm long) was projected into the enclosure through a small slit in the aluminium tape, such that the bead was in the centre of the enclosure, directly above the copper tube injecting fuel. The probe was held in place by a robotic traverse mechanism, which was also used to change the vertical position of the probe. Measurements were made at intervals of 5 mm, starting 5 mm above the water surface. Since the height of the blue whirl changes continuously,

the height of the probe above the water surface was measured, rather than different regions of the blue whirl independently.

Thermocouples of 50 μm wire diameter were used as they provided accurate measurements (based on [42], ±5 K in this study) and quick response times (~0.02 s). Data was recorded using a data-acquisition system (NI cDAQ-9171 bus with NI TB-9214 terminal block) at 100 Hz. The continuous movement of the whirl within the enclosure caused intermittent interactions of the blue whirl with the thermocouple bead. Thus, experiments were recorded using a high frame rate (HFR) digital camera (Casio EX-F1) at 300 fps to capture the formation and movement of the blue whirl during the experiment. The video was focused on the region around the thermocouple bead, and was used to determine the time periods when the thermocouple bead was in direct contact with the flame, indicated by a glowing bead.

Before lighting the fuel pool for each test, the flame from the butane torch was placed momentarily over the thermocouple bead to record a spike in the temperature data log. This spike served as a marker to synchronize time stamps of the HFR video with that of the raw thermocouple data log. Experiments were generally repeated three to five times depending on the number of interactions of the blue whirl with the thermocouple bead. Measurements at each vertical location were recorded for over three minutes. Only experiments when the blue whirl was steadily sustained for over three minutes were used for data analysis. This ensured a sufficient number of interactions of the blue whirl with the bead. Temperatures for a maximum height of 75 mm above the water surface are reported here, beyond which the continuous contortion

of the purple haze made it challenging to visually determine whether the thermocouple bead was interacting with the blue whirl.

In order to improve the accuracy of measurement, a 75 μm thermocouple was also used to obtain measurements at the same vertical locations, such that a radiation correction could be applied, following the work of Singh and Gollner [43]. A system of two equations (*Eqns. 1 and 2*) with two unknowns, T_g (gas temperature) and U (flow velocity) represents the thermal balance for each thermocouple. Usually an iterative procedure is required to solve these as kinematic viscosity and thermal conductivity are functions of temperature. However, to make the solutions simpler, kinematic viscosity and thermal conductivity were assumed to be constant, such that iterations were not required to solve these equations simultaneously.

$$T_g - T_{tc1} = \frac{\varepsilon_{tc1}\, d_{w1}\, \sigma}{k\left[0.24 + 0.56\left(\frac{U d_{w1}}{\nu}\right)^{0.45}\right]}\left(T_{tc1}^4 - T_{surr}^4\right) \qquad \textit{Eqn. 1}$$

$$T_g - T_{tc2} = \frac{\varepsilon_{tc2}\, d_{w2}\, \sigma}{k\left[0.24 + 0.56\left(\frac{U d_{w2}}{\nu}\right)^{0.45}\right]}\left(T_{tc2}^4 - T_{surr}^4\right) \qquad \textit{Eqn. 2}$$

The procedure involves using the average temperature obtained from each thermocouple at a height of 10 mm above the water surface, and *Eqns. 1 and 2* were solved to obtain the local velocity. Once the velocity was evaluated, each of the equations turns into independent single variable equations that can be directly manipulated to obtain the gas temperature, T_g. This velocity was then assumed to be constant at all heights, and could thus be used to correct temperatures obtained from just one thermocouple (50 μm) at all heights. This further simplifies the procedure as simultaneous solutions to *Eqns. 1 and 2* were needed only once. Using this procedure,

the maximum radiation correction applied to the 50 μm thermocouple measurements of the blue whirl was 109 K.

3.3 Thin-Filament Pyrometry

Thin-filament pyrometry was used to obtain a 2-dimensional (radial and vertical/axial) temperature distribution of the blue whirl. Past studies have utilized this technique in many different combustion systems [44–48], as well as soot pyrometry [49]. The general concept involves thin SiC filaments (usually ~15 μm in diameter) strung across a flame, images of which are captured using a camera. The images are then post-processed to identify luminosity of the filament at a pixel level. A calibration to relate the luminosity of the filaments to temperature is performed using either a standard flame or numerical evaluation. Using the calibration, the filaments can then be used in other configurations, and filament luminosity can be used to derive local temperatures (refer *Figure 45* for procedure schematic). Although multiple investigations have been conducted utilizing TFP in combustion systems, to the best of the author's knowledge, this study employs the most number of filaments used simultaneously for instantaneous measurements. A simple approach, similar to [50,51] using a digital camera is followed here. Suitable changes in the approach were made to make the technique suitable for implementation within the constraints of the experimental setup.

HI-NICALON^{TM} filaments (manufactured by Nippon Carbon Co., Ltd. (NCK), Japan, and supplied by COI Ceramics, Inc.) were used due to their low oxygen content (wt % Si:C:O :: 62:37:0.5) and high thermal stability that allowed longer test periods.

Individual filaments were suspended on either side of the enclosure to vertical uprights by means of tape (*Figures 14 and 15*). Filaments (60 mm in length) were stretched across the enclosure such that they passed through the small gap between the two quartz half-cylinders, to form a 2D filament array. A total of 11 filaments were used – one every 10 mm up to a height of 10 cm above the water surface, and one at 5 mm above the water surface. The filament at 5 mm was used to specifically probe temperatures in the blue cone (refer *Figure 44* in the *Appendix*). Once in place, the filaments were heated using a propane torch before each experiment. This surface treatment was found to remove the surface coating and any soot deposited on the filaments [50,51]. The tautness of the filaments was controlled through a simple mechanism that permitted small movements of the upright (*Figure 15*).

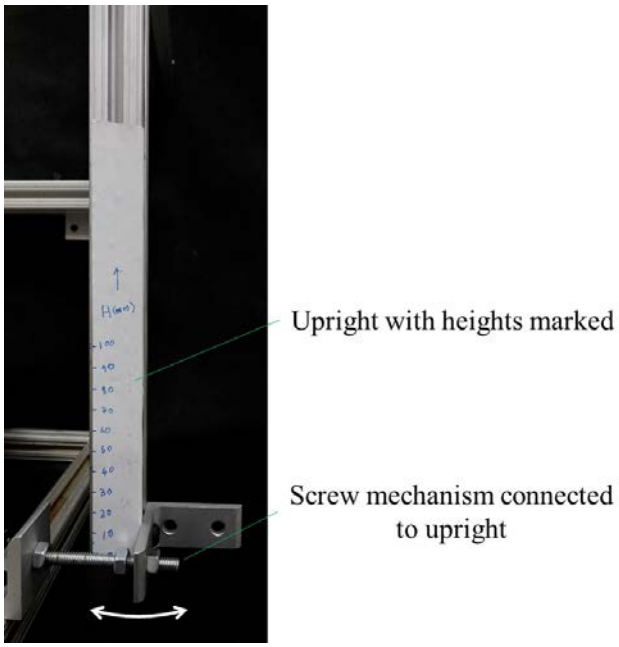

Figure 15. Image of experimental setup showing mechanism to control filament tautness.

A Nikon D7100 camera body with an aspherical lens (DX AF-S Nikkor 18–105 mm 1:3.5-5.6G ED) was used for capturing images of the filament array. The camera was operated in full manual mode at *f*/5.6, ISO 500 and 1/1600s shutter speed, providing a temporal resolution of 0.625 ms and a depth of field of ~6.5 mm. The high shutter speed prevented saturation of RGB planes and provided good temporal resolution. C_H mode (6 fps) was used to continuously capture images when the blue whirl interacted with the filament array. The camera was operated between a focal length of 30-32 mm, giving a spatial resolution of ~29 μm/pixel.

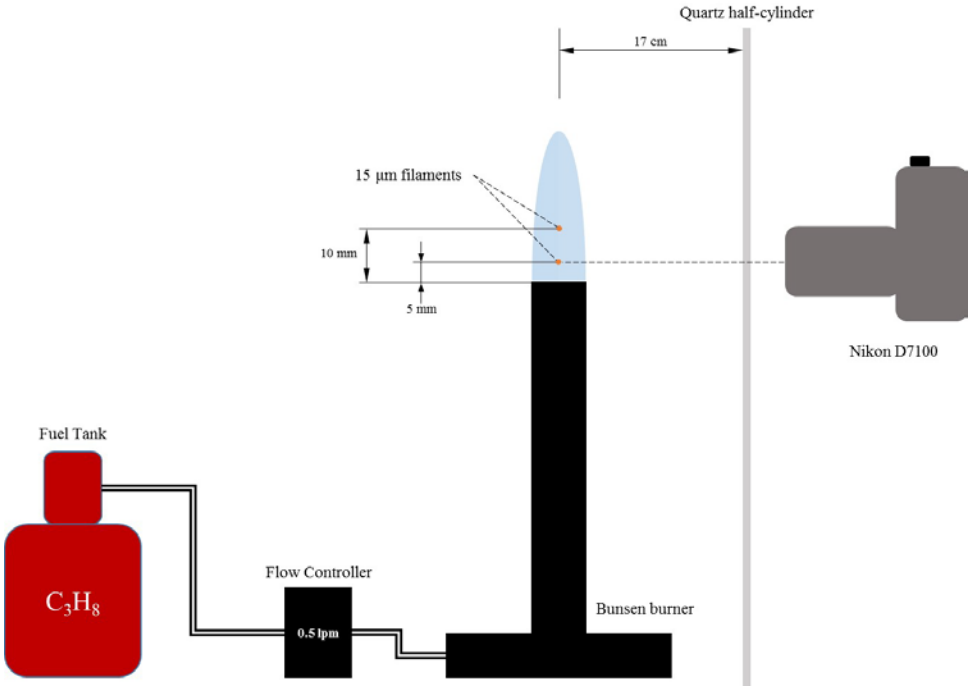

Figure 16. Schematic of TFP calibration setup.

The calibration setup (*Figure 16*) consists of 20 cm long filaments suspended across a stand placed over a Bunsen burner. Propane was supplied to the Bunsen burner at 0.5 L/min. Two filaments were positioned 5 mm and 10 mm above the burner exit.

The camera was operated at 105 mm focal length, resulting in a spatial resolution of 21.55 μm/pixel (compared to 42 μm/pixel in [51]). The better spatial resolution stems from the higher pixel density of the camera sensor, although the camera was farther away. Since images of the glowing filaments over the blue whirl needed to be captured behind the quartz half-cylinder, the quartz half-cylinder was used in the calibration setup as well, to reproduce actual experimental conditions, ensuring accurate calibration. The distance between the quartz half-cylinder and the filaments was the same in the calibration setup and the blue whirl setup. Images of the filaments over the Bunsen burner (*Figure 17*) were captured using a remote shutter trigger.

The Bunsen burner was operated in premixed mode without the production of any soot, providing reliable thermocouple measurements up to the middle of the flame. Beyond the central axis of the burner, the thermocouple probe was observed to affect the flow field out of the burner, resulting in a reduced number of usable data points for correlation with filament intensity. The temperatures of the Bunsen burner flame were recorded using 75 μm and 125 μm thermocouples at the two different heights on one side of the flame. Measurements were made every 0.2 mm for 30 seconds, starting from the centre of the burner exit up to a distance of 12 mm away from the centre, where ambient temperature conditions were observed. Accurate movement was achieved using the robotic traverse mechanism. The traverse mechanism and DAQ were the same as described in section *3.2*. The thermocouple measurements within the Bunsen burner flame required a maximum temperature correction of ~200 K, with an estimated uncertainty of ~80 K.

Figure 17. An image of the filaments positioned across a Bunsen burner flame for calibration.

Experiments and calibration for TFP were conducted in complete darkness, with all lights in the laboratory turned off. All images were recorded in NEF RAW format (large size, 6000 x 4000 pixels) in Adobe Colorspace, and converted to TIFF using Nikon ViewNX-i software without any compression. The image was then imported into Spotlight-16 [52], where the line profile tool was used to obtain 12-bit grayscale luminosity values (average of RGB 12-bit values) across the filaments. A line width of 8 pixels perpendicular to the glowing filament was used to account for the apparent increase in luminosity compared to the non-luminous widths of the filaments.

Filament luminosity was averaged over 5 pixels (parallel to glowing filament) every 0.2 mm to obtain the pertinent weighted grayscale value at the particular locations. These were then matched with the radiation corrected thermocouple-derived gas temperatures at the corresponding locations. The spatial luminosity data was

correlated with the radiation corrected thermocouple temperature data based on the spatial resolution of the images. Spatial resolution was measured by placing a scale at the object plane, and using the line profile tool in Spotlight-16 to measure the number of pixels in the image for a given length between calibration marks on the scale.

The resulting temperature vs. grayscale luminosity plot (*Figure 18*) was observed to follow a two term exponential behaviour, with an R^2 value of 0.95, and followed a trend similar to that obtained by Maun [50]. The calibration curve was determined to be valid up to a maximum pixel intensity of 4095, which translates to a temperature of ~2105 K. Since the flow field of the blue whirl is not known a priori in this study, radiation corrections are performed only on thermocouple measurements of the calibration flame. The measurements obtained through this method are sufficiently accurate, considering the relatively small axial velocities expected within the small flame. When sufficient information about the flow-field is available in the future (through simulations or detailed measurements), a new calibration may be used to re-evaluate temperatures, although no qualitative change of results are expected. The fit function is a two term exponential of the form

$$f(x) = ae^{bx} + ce^{dx}$$

with the values of coefficients presented in *Table 1*.

Table 1. Coefficients for two term exponential calibration function.

Coefficient	Value	(95% CI)
a	1127	(971.8, 1282)
b	0.0001526	(0.0000983, 0.0002069)
c	-1020	(-1260, -780.1)
d	-0.01537	(-0.02252, -0.008218)

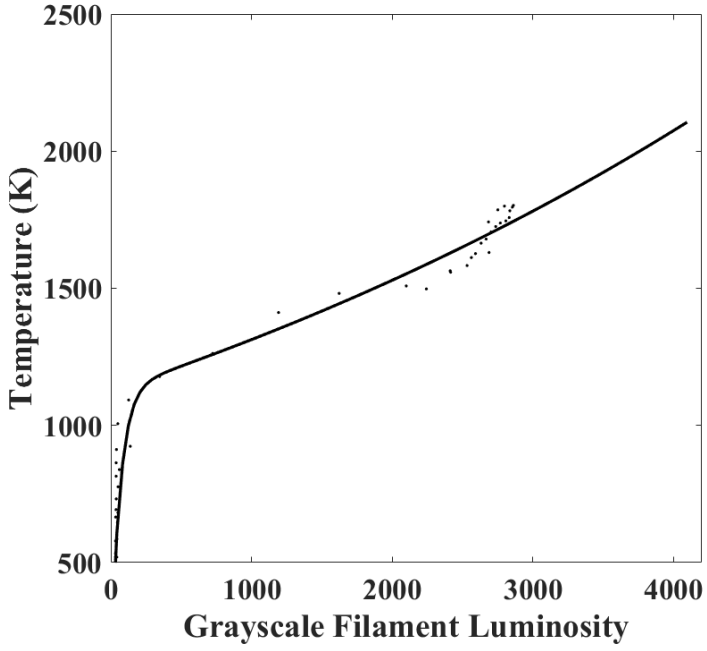

Figure 18. Calibration profile of filament intensity as a function of temperature.

The calibration curve may be considered to be linear beyond 1200 K. Background luminosity levels were observed to be very close to zero, and the calibration range is 500 – 2105 K, beyond which pixel saturation occurs. The temperature resolution of the system is ± 0.226 K per unit grayscale intensity, similar in behaviour to [51]. Small differences may be attributed to the different filament material, burner and camera used to perform the calibration.

3.4 OH* Spectroscopy

Optical spectroscopy of various radical species has been used in combustion systems to identify various properties of a flame locally, such as equivalence ratio [53][54], and heat release rate [55]. These techniques have also been used to design

practical engineering systems [56,57]. The presence of these radicals has even been used in numerical simulations to derive local flame conditions and properties [58][59][60]. The presence of OH radicals in a combustion reaction is a major determinant of the reaction rate, and a sufficient steady-state concentration of these radicals may even result in an effective explosive condition [61]. OH* radicals are at higher energy levels than the OH radical, and the ultraviolet bands of OH* during de-excitation to ground state is in the neighbourhood of 3100 Å [62].

Qualitative OH* spectroscopy was performed in this study to identify the reaction front in the blue whirl using a 10 nm band-pass filter centred at 307 nm. The filter was used in a lens (UV-Nikkor 105 mm 1:4.5) mounted on an intensified CCD UV camera (Xybion ISG-250-GQU). The camera was positioned with a horizontal view of the blue whirl, such that all three distinct regions were visible with minimal overlap, and the frame was mostly occupied by the blue whirl. Video of the development of the blue whirl was captured at 30 fps and recorded through an analogue-to-digital converter (Elgato video capture) using a composite RCA cable.

With the aperture at *f*/5.6, the gain level was adjusted to prevent pixel saturation. A similar procedure was repeated for the yellow fire whirl, but with the camera positioned farther away such that the entire fire whirl was visible within the frame. Selected portions of the videos, showing the blue whirl and fire whirl were extracted as image frames (.tif). The RGB planes were extracted from these images and converted to grayscale in MATLAB as a weighted average of RGB values (0.2989R + 0.5870G + 0.1140B). The grayscale values represent spatial distribution relative concentrations of the OH* radical, revealing qualitatively where in the image the reaction is generally

occurring. The values presented here are not indicative of absolute species concentrations.

3.5 Surface boundary conditions for formation

To investigate the effect of the bottom surface boundary on the formation of the blue whirl, conditions other than the water surface were also used to observe the temporal evolution of a fire whirl. The different configurations are specified in *Table 2* and depicted in *Figure 19*. The conditions considered here mimic typical configurations used in laboratory studies of fire whirls (fuel pans with lips, or fuel soaked wicks), to study their effect on the formation of the blue whirl, and attempt to explain why, despite extensive study, the blue whirl regime has not been observed until now. To identify whether the formation of the blue whirl was unique to just the water surface (i), different surface materials – a metal plate (ii), and a porous ceramic fibreboard (iii) were studied. These configurations (i-iii) were continuous, flat and unimpeded surfaces (*Figure 19a*). Two different fuel pan configurations (iv and v), both with lips were studied to observe the effect of the pan lip (*Figures 19 b and c*). The apparatus was the same in all other aspects, and small variations of slit width and enclosure positioning were attempted by trial and error in order to identify if a stable blue whirl could be formed. Digital images of the evolving whirls were captured in each configuration.

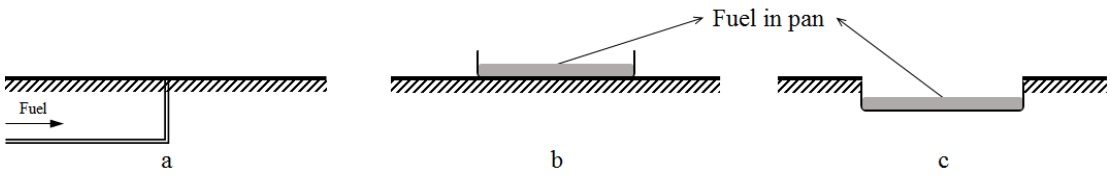

Figure 19. Schematics for the different surface boundary conditions as described in *Table 1*. Conditions (i-iii) are represented by (a), (iv) by (b), and (v) by (c).

Table 2. Different surface boundary conditions studied for their effect on the formation of the blue whirl.

	Surface Boundary Condition	**Schematic**
(i)	Water surface	*Figure* 19*a*
(ii)	Smooth stainless steel surface	*Figure* 19*a*
(iii)	Porous ceramic fibre surface	*Figure* 19*a*
(iv)	Fuel dish over the steel surface	*Figure* 19*b*
(v)	Fuel dish embedded beneath porous ceramic sheet	*Figure* 19*c*

Chapter 4: Results

This chapter presents the results of the digital images captured and the various diagnostics implemented on blue whirls generated under various experimental conditions. The physical structure, thermal structure and details of the reaction front are presented in order, followed by the surface boundary conditions required for the formation of the blue whirl.

4.1 Visual characteristics of The Blue Whirl

Upon ignition of fuel within the enclosure, a pool fire was observed to form. When a small pool of fuel (~2.5 ml) over water was ignited, the fuel pool was observed to spread out during the formation of the pool fire. The pool fire (flames ~15 cm in height) was observed for ~2 s before a traditional yellow fire whirl began to develop. The height of the fire whirl then increased to around ~70 cm, while accompanied by significant aural indications suggesting that increasing entrainment was occurring.

The development from a pool fire to a fire whirl in the setup used for this study is shown in *Figure 20*. Different stages, such as the inclined whirl, as described in [15] and [16], were also observed prior to formation of the fire whirl, but generally for short durations. The large traditional fire whirl (~80 cm) then proceeded to continuously decrease in height, and a conical fire whirl (*Figure 21*) that "danced" over the water surface was formed [4]. The conical whirl is similar in appearance to *Fig. 3f* in [16], and the base of the whirl was blue, similar to *Figs. 4d-4f* in [16]. Aural indications due to increased entrainment have previously been reported during the formation of a conical fire whirl, even when using rotating mesh apparatus, and may be considered as

an indication of a turbulent boundary layer [16]. The base of the conical fire whirl (*Figure 22a*) was observed to be slightly above the fuel surface, and the whirl showed precession within the enclosure. However, the base of the larger yellow fire whirl (*Figure 22b*) did not appear detached from the fuel surface, and was not observed to show significant precession at the base.

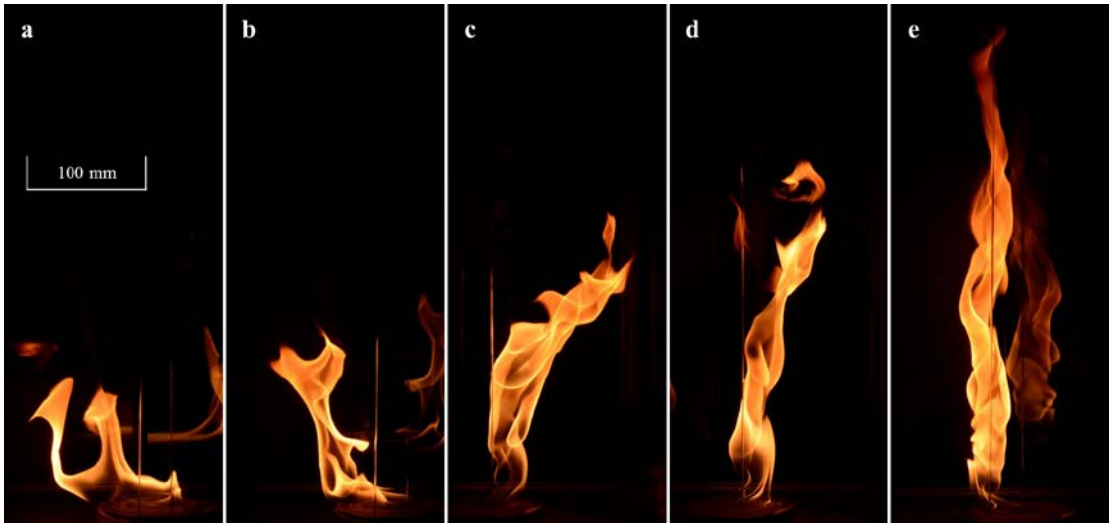

Figure 20. Development of a fire whirl. Reflections off the quartz setup used are also visible.

Figure 21. Different forms of the conical whirl formed over a water surface.

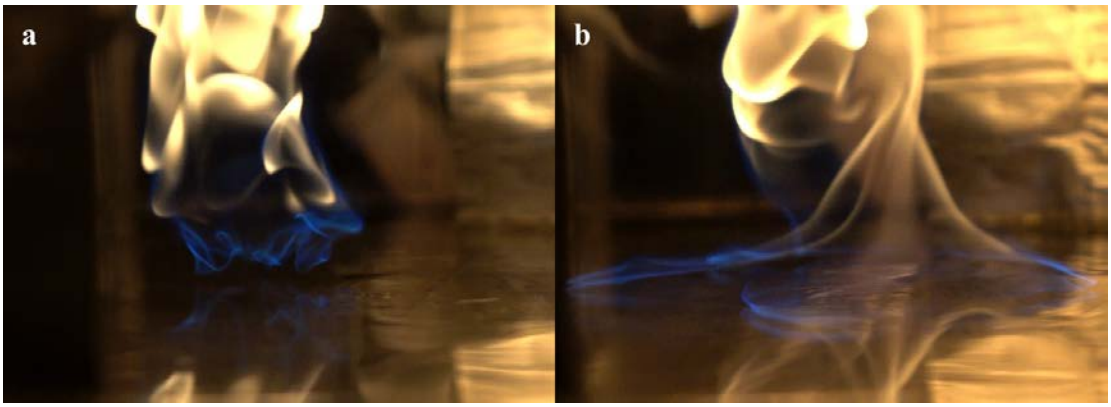

Figure 22. Comparison of fire whirl base above the fuel surface in (a) Conical fire whirl, (b) Traditional yellow fire whirl.

The lower blue region of the conical whirl, directly above the fuel surface then lifted up to form a structure that resembled an inverted blue cone. Once stable, aural signs reduced and a completely blue flame was observed to constantly exist, with no visible yellow light from the flame. The blue cone was also observed to sit a small distance above the fuel surface [4].

The physical structure of the blue whirl is comprised of three distinct regions – the lower blue cone, the bright vortex rim, and the upper purple haze, as depicted in *Figure 23*. The flame was observed to show precession around the centre of the enclosure over the water surface, similar to the conical fire whirl that the blue whirl evolved from. The height of the blue cone varied between 1 and 2 cm. The size of the whirl was observed to constantly change – when fuel supply was stopped, it was observed to retain its shape and structure, but continuously diminish in size until extinction.

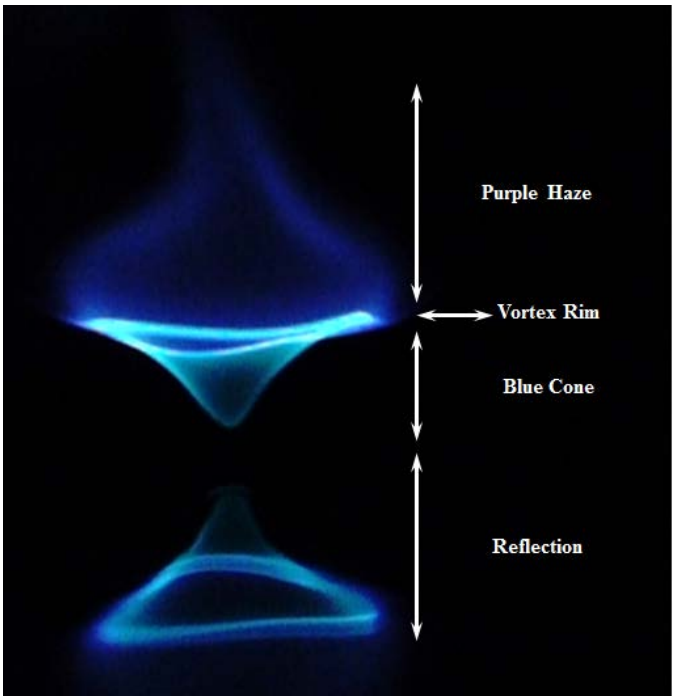

Figure 23. Blue whirl with different regions indicated.

As long as the fuel was supplied at a constant rate, the blue whirl was observed to exist continuously [4]. These long stints of the blue whirl were observed to "flicker" intermittently at times into small luminous laminar flames that immediately transitioned back to the blue whirl structure. These luminous laminar whirls were similar in structure to the conical fire whirl (*Figure 21b*). The circular blue edge at the base of this luminous flame (also visible in *Figure 21b*) lifted up to form the vortex rim of the blue whirl. The transition to a perfect blue whirl was sometimes observed to take multiple attempts of the lower blue portion lifting up to form the blue ring. The development of the blue whirl from the laminar conical whirl is depicted in *Figure 24*.

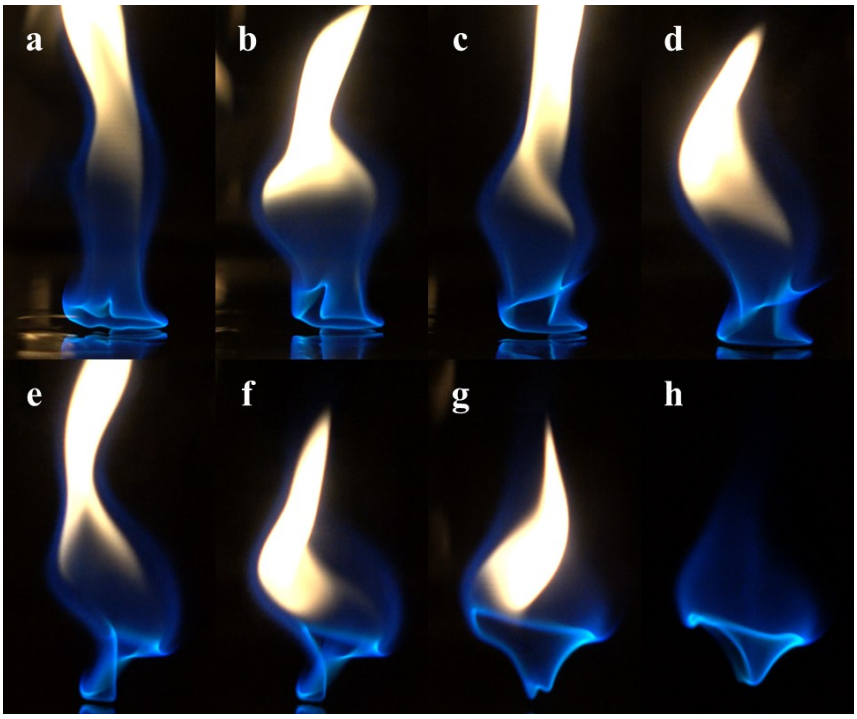

Figure 24. Transition from a laminar conical fire whirl to a blue whirl (~1.5 s).

Both the traditional yellow fire whirl and blue whirl were observed to concentrate fuel over the water surface towards the centre of the enclosure, although occasionally the fuel pool area was discontinuous. The water surface and fuel were also observed to show swirl in the same sense as the vortex within the enclosure. When water in the pan was not replaced after many tests, dark viscous liquids, presumably impurities in the fuel were observed to collect over the water surface. These globules floated on the water surface, and reduced the swirl on the water surface. This reduced swirl was not visually observed to alter the stability of the blue whirl. Thus, it is as yet unclear whether the swirl of the water below affects the blue whirl's formation, or stability.

At times, only a portion of the blue cone was seen to show precession over the water surface, and then revert to the cone shape, a sequence depicted in *Figure 25*. This partial cone flame sometimes resulted in flame extinction, and sometimes a reversion to the full cone shape.

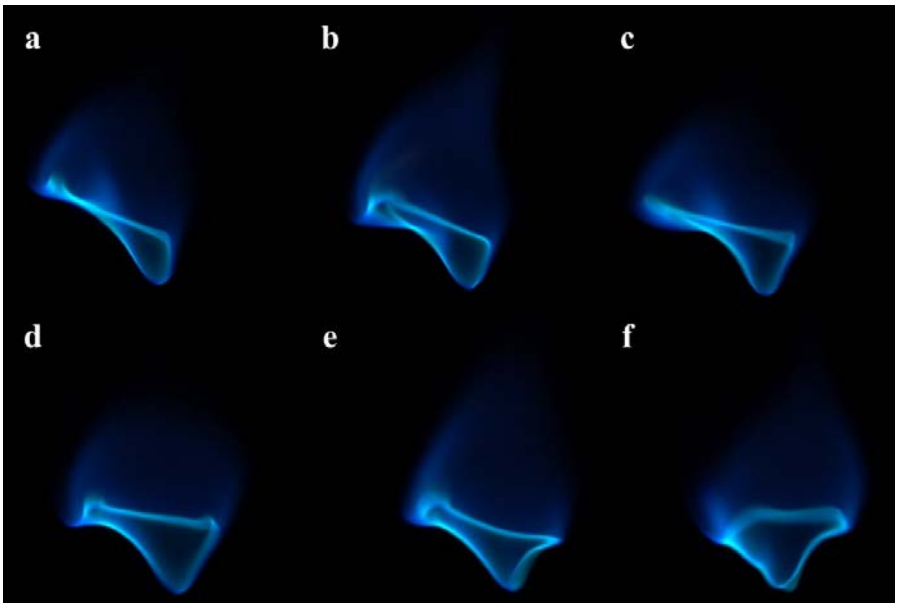

Figure 25. Reversion of a partial blue cone to a full blue cone.

The transition to a blue whirl was observed to show interesting patterns of soot streaks within the whirl (*Figure 26*). Sometimes, single soot particles were seen to emanate from the vortex rim and leave the flame through the purple haze (*Figure 1b*). Although some recirculating motion can be seen in *Figure 26b*, the directions are not immediately apparent. Since it was postulated that the blue whirl may correspond to a reactive bubble mode of vortex breakdown [4], identifying flow directions within the blue cone may help confirm the analogies, and the role of vortex breakdown in determining the shape of the whirl. However, seeding the flow with foreign particles was not possible due to the presence of the water surface, and smoke visualizations

seemed to destabilize the blue whirl, causing a reversion to the conical whirl. Thus, the recirculation directions were identified using high frame rate videos of transition events, and observing flow patterns of the yellow soot particles.

High-frame rate videos were captured using a Sony RX10 II at 960 fps in quality priority and “End Trigger” modes, providing 40x slow motion playback. The soot particles revealed a recirculating pattern during transition events from the yellow conical fire whirl to the blue whirl. A sequence of images obtained from one such video in a space of ~20 ms is shown in *Figure 27*. In the event of a successful formation of the blue whirl from a transitional whirl, soot particles tend to either get consumed within the blue cone region, or exit the blue cone in the axial direction.

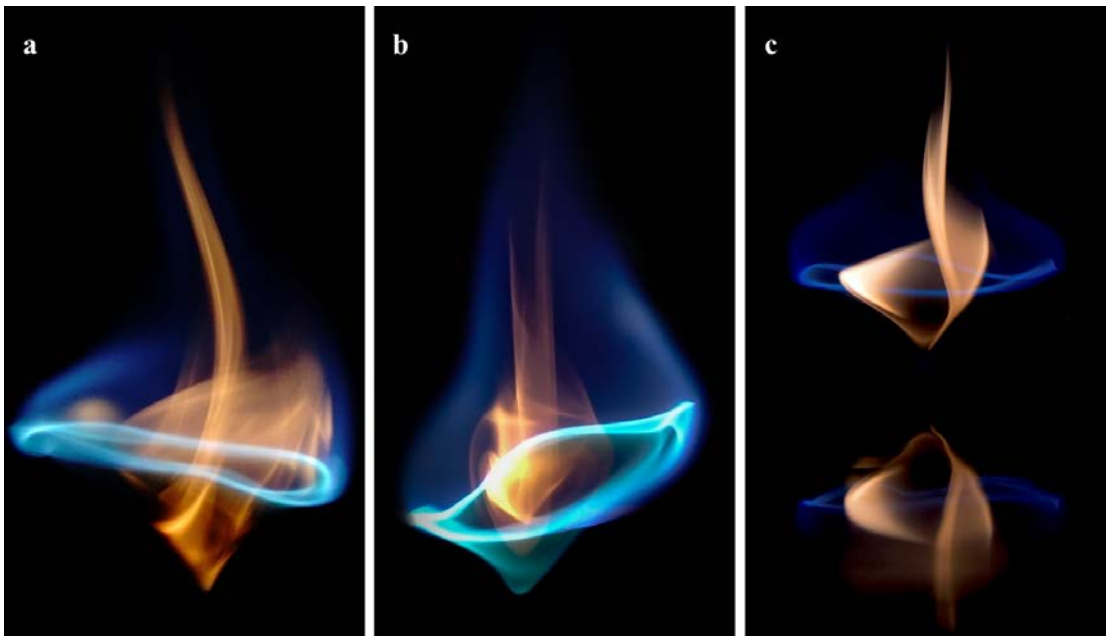

Figure 26. Blue whirls captured during transition, revealing recirculating patterns of soot within the blue cone.

The blue cone also resembles a hard boundary, preventing soot from passing across the flame sheet of the blue cone. This is visibly evident in *Figure 26a*, where the

presence of the soot may be used to identify the boundary of the lower blue cone. In general, the recirculating patterns show some similarity to the bubble mode, with the lower base of the blue cone being analogous to the upstream end of the breakdown bubble. The video also revealed that downward fluid motions filled the blue cone, and soot exited through the purple haze region, causing emptying of the blue cone. Similar behaviour has been found in vortex breakdown bubbles [35,37]. However, as evident from *Figure 27*, the motion of the soot particles within the blue cone is quite complex due to the 3-dimensional nature of their motions. A 2-dimensional video cannot fully capture the complex motions within the different regions of the blue cone. Therefore, generalizations cannot necessarily be made without more detailed study. Based on the structure of the breakdown bubble (either Type 0 or Type 1, depending on stability), the flow may also include a stagnation zone, if the blue cone is indeed representative of the bubble mode vortex breakdown.

It has been proposed that the cylindrical fire whirl (with visual features similar to *Figure 1a*) is formed from a conical whirl due to a flame instability induced by vortex breakdown [16], with a disturbance travelling down from the flame tip towards the fuel source. In the setup used for this study, a similar behaviour was observed, but during a transition from a conical fire whirl to a blue whirl, with visible soot particles travelling down towards the fuel pool (into the blue cone), before forming a part of the recirculation present within the blue cone. These downward motions are not immediately evident from the individual frames in *Figure 27*, but can be seen in the video that these frames were extracted from.

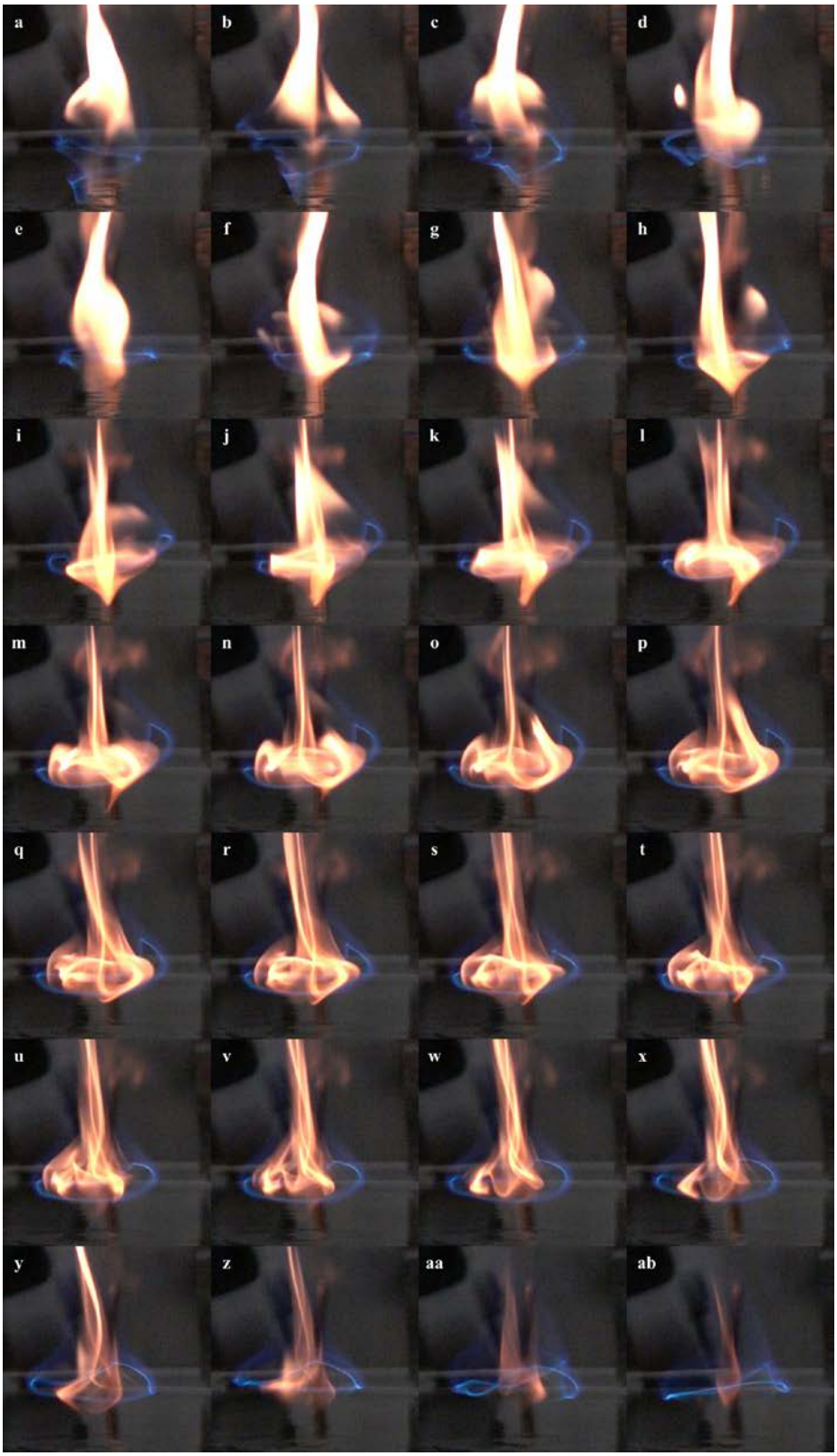

Figure 27. Images extracted from HFR video revealing recirculating motions within the blue whirl (~20 ms).

4.2 Vertical Temperature Distribution

Temperatures recorded using thermocouples were extracted from the temperature log based upon the time stamps provided by the video. At each height, approximately 1700 different measurements were averaged, and a radiation-corrected temperature was obtained using the procedure outlined in [43]. These are represented as a vertical temperature distribution in *Figure 28*, with error bars indicating a 95% confidence interval. Although the height of the blue whirl does not remain constant, the different regions are marked based on general observations during steady presence of the blue whirl. The maximum temperature is obtained as an average of the top 5% of the temperature measurements. Since the blue whirl constantly moves in and out of the vicinity of the thermocouple bead, the maximum temperatures are a useful estimate of the peak values until a better non-intrusive diagnostic can be implemented.

The temperature can be observed to generally increase with height in the blue cone, which has lower temperatures than the purple haze. The peak temperatures of the blue whirl were generally lower than 1500 K, but the purple haze can be seen to peak at ~2000 K, which is higher than expected for a non-premixed n-heptane flame [63].

The thermocouple probe was observed to destabilize the blue whirl during some interactions, especially when interacting with the blue cone. The destabilization caused the flame to turn into a small luminous laminar conical whirl, but was observed to be less problematic when the probe interacted with the region of the blue whirl above the vortex rim.

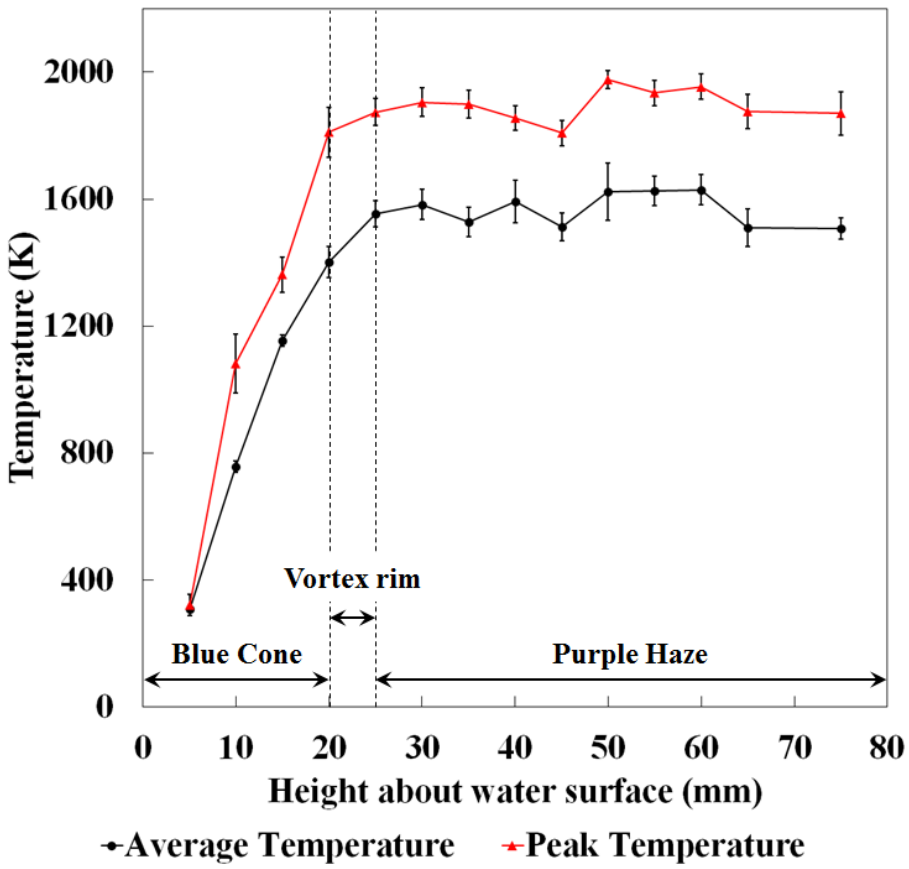

Figure 28. Vertical temperature distribution of the blue whirl when formed over water, from 50 μm R-type thermocouple measurements.

4.3 2-Dimensional Temperature Distribution

A blue whirl, in its "perfect state," is radially self-similar, and thin-filament pyrometry provides a 2-dimensional temperature distribution in one radial plane. Flame and plume tilting and contortion resulted in varying levels of the blue whirl interacting with the filament array. The tilting meant that the radial plan of the blue whirl may not be parallel to filament plane during interaction, thus resulting in varying levels of blue whirl interaction with the filament array at a given time. Due to the larger width and relatively smaller movement of the blue cone as compared to the purple haze, the lower

filaments had wider glowing sections. The blue whirl formed using heptane and the glowing filaments above it are shown in *Figure 29a* (captured at 1/50 s and ISO 1250). The lowermost filament at 5 mm above the water surface was observed to glow in very few images – one such instance is visible in *Figures 29 a and b*.

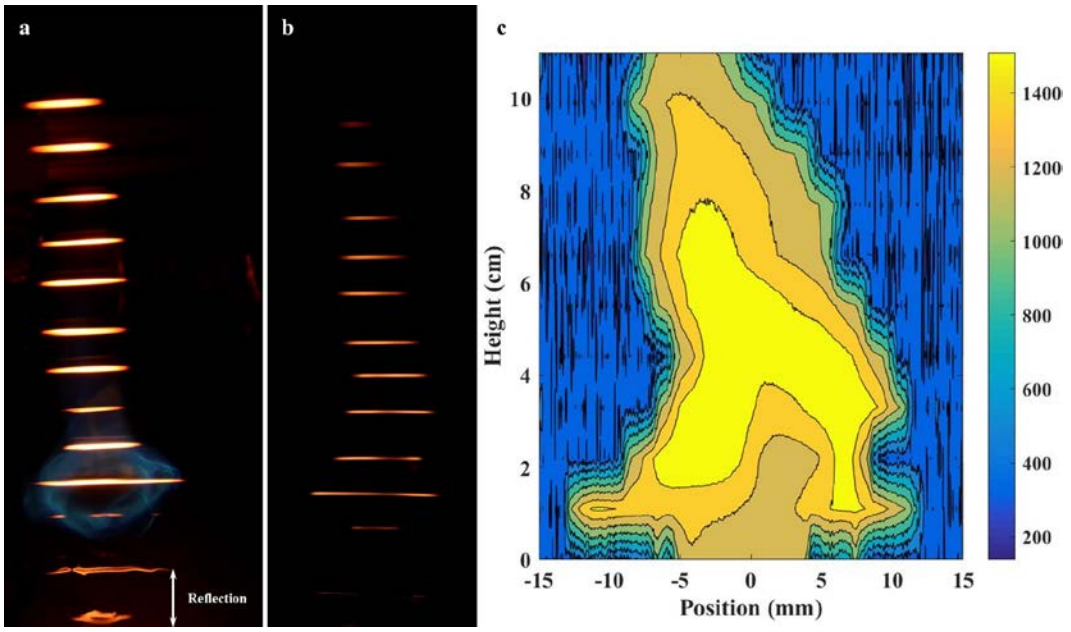

Figure 29. (a) Glowing filaments with blue whirl formed using n-heptane over water, (b) Actual instantaneous TFP image, (c) Instantaneous temperature contour.

A slight yellow nature in the height range of 20-50 mm was sometimes visible to the naked eye, which may be from soot particles. However this has not been captured on any image, suggesting they are not at very high temperatures. This may be attributed to the cooling effect produced by the filaments during these interactions. The reflection of the lowermost filaments on water are visible only at lower shutter speeds, and are thus not observed when captured at calibration settings (*Figure 29b*). The instantaneous temperature map obtained from *Figure 29b* is represented in *Figure 29c*. The general structure of the contour map is similar to the visually observed features in the image

obtained directly from the camera. The hottest region can be seen in the purple haze, above the blue cone. The filament at 1 cm can be seen to show high temperatures at the ends, which may correspond to an interaction with the vortex rim, though the axial resolution (determined by filament spacing in the axial direction) is not sufficient to determine whether higher temperatures might be obtained within the vortex rim.

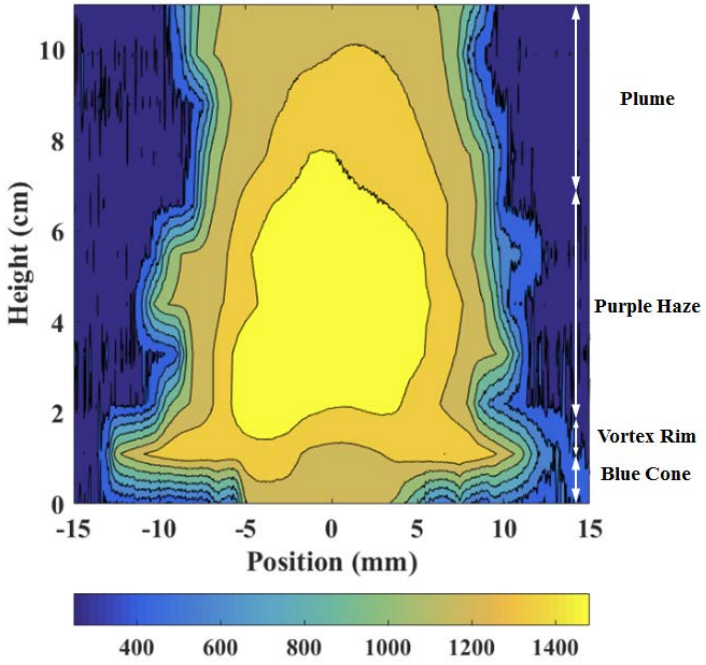

Figure 30. Average temperature map of blue whirls formed using heptane over water.

An average temperature map (*Figure 30*) was obtained from 5 different images of the filament array over whirls generated using n-heptane. To keep the averaging technique from "smearing" the instantaneous data, care was taken to select images that were centred along the same point, although there was still some movement and tilting of the whirl. This is similar to the technique performed by Hartl and Smits for PIV data [9], where their data was taken along the centre of a fire whirl core to ensure more accurate velocity measurements. A visual correction was also performed by Emmons

and Ying for temperature data [3]. The average temperature obtained through TFP (*Figure 30*) at each filament position is plotted as a function of radius in *Figure 31*.

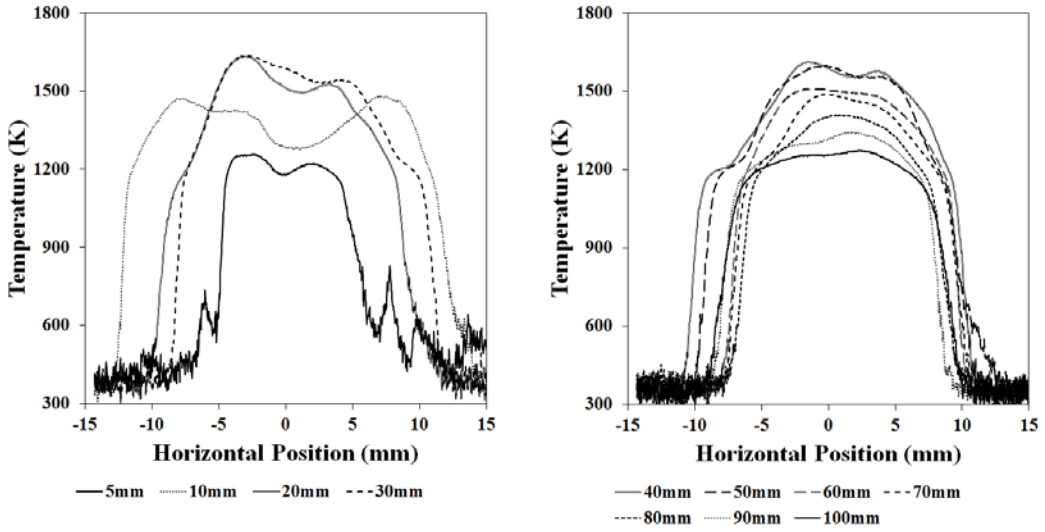

Figure 31. Average temperature profiles as a function of radius at selected heights above the water surface.

The temperature of the lower blue cone remains lower than 1500 K. Although the vortex rim is hotter than the blue cone, the region of the whirl immediately above the rim (the purple haze) is the hottest, above ~1600 K. Above 6 cm, the temperature begins to decrease, indicating that there is no further heat release, and may be considered to be in the plume region. The radial distribution of the blue cone is similar to results from [3] (shown in *Figure 3*), with a hump-like temperature profile up to ~20 mm above the water surface. This may suggest that the sheet formed by the blue cone is analogous to the edge of the vortex core of a traditional yellow fire whirl, based only on temperature measurements. Consequently, the flame sheet of the blue cone may also be the region of maximum tangential velocity.

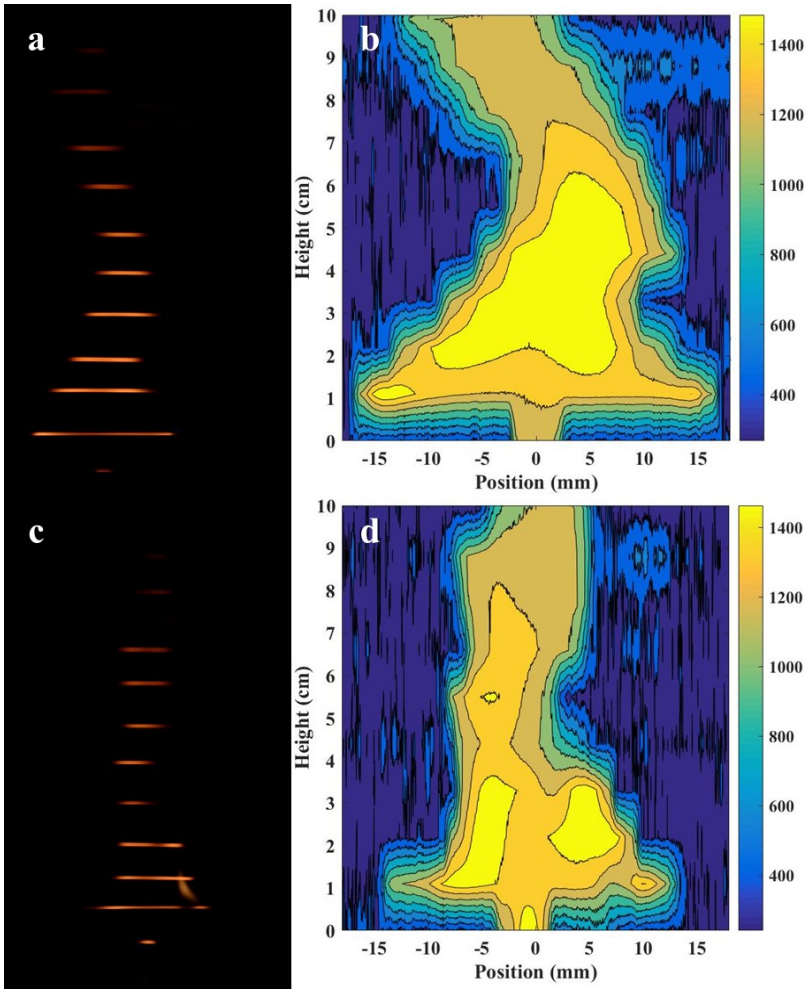

Figure 32. Instantaneous TFP images of blue whirls formed over water using (a) iso-octane and (c) cyclohexane. Corresponding temperature contours are shown in (b, d).

Table 3. Volumetric supply rates for different fuels used to form a stable blue whirl in this study.

Fuel	Supply rate (ml/min)
Heptane	1.1
Iso-Octane	0.95
Cyclohexane	0.7
Acetone	1.8
Ethanol	2

Thin-filament pyrometry was repeated for two different fuels – iso-octane and cyclohexane. The cylinder slit widths were maintained constant, and fuel supply rates

were altered by trial and error to account for the lower rate of burning of these fuels. The supply rates for the different fuels used in this study are presented in *Table 3*. The instantaneous temperature contours obtained through thin-filament pyrometry for iso-octane and cyclohexane are shown in *Figure 32*.

The technique was performed for blue whirls generated over a metal surface as well. Replacing the water pan with a flat aluminium plate, fuel was supplied through a small hole such that the surface was even without undulations. With a filament array over the metal plate, blue whirls were created with different fuels over the metal surface. In addition to heptane, iso-octane and cyclohexane, acetone and ethanol were also used. Acetone and ethanol were used only over the metal surface due to their miscibility with water. The images and corresponding temperature contours of blue whirls formed over the metal surface are depicted in *Figure 46*. Qualitatively, these contours are similar to blue whirls formed over water. Slight differences in the instantaneous thermal structure arise from varying levels of interaction of the blue whirl with the filament array. The high temperature region appears to occur at a lower height for whirls formed using acetone and ethanol compared to other hydrocarbons used in this study.

The instantaneous temperature contours presented in *Figures 29, 32 and 46* share a similar thermal structure irrespective of the fuel, with a distinct vortex rim, a higher temperature portion above the vortex rim, and a lower temperature region below the vortex rim. And, for a given fuel, the distribution is not very different whether formed over water or the metal surface. However, it is apparent that the vortex rim region occupies a higher axial position when the blue whirl is formed over the metal

surface than the water surface. This may be attributed to the higher thermal conductivity of the metal surface.

4.4 Reaction front through OH* Spectroscopy

Video was recorded from an intensified CCD camera (described in *Chapter 3: Experimental Method*) using an analogue to digital converter connected directly to the camera. Then, frames of the blue whirl and yellow fire whirl were extracted (in .tif format). These were converted to grayscale luminosity in an 8-bit scale to obtain a contour plot, represented in *Figure 33*. A single frame from each of the videos (*Figures 33a and 33c*) shows the grayscale image of spatial OH* concentration. To visualize contours of the relative luminosity, contour plots of these images were generated using the "rgb2gray" command, and are shown in *Figures 33b and 33d*.

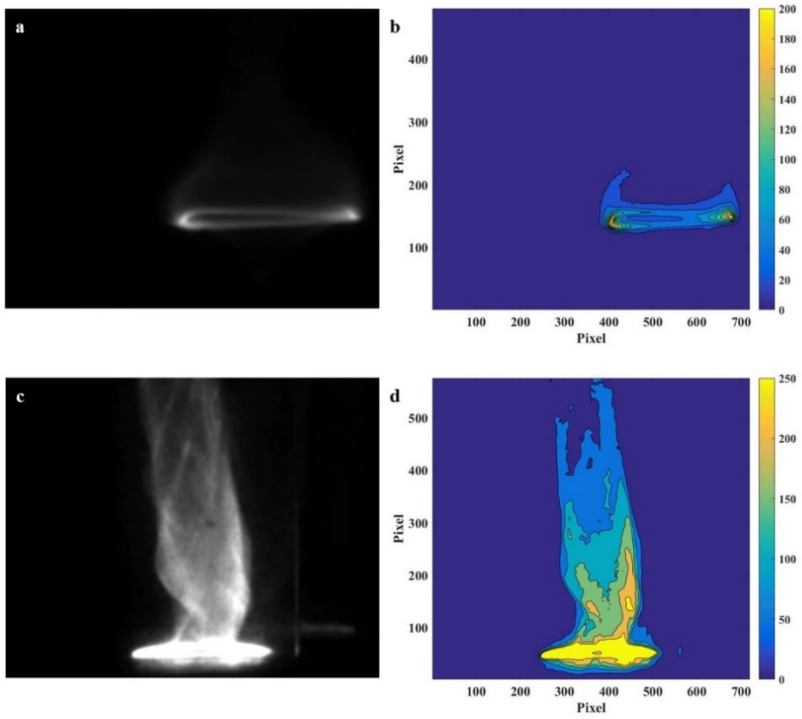

Figure 33. Comparison of OH* chemiluminescence in (a) blue whirl and (c) yellow fire whirl and corresponding luminosity contours (b, d).

In contrast to the structure visible to the eye, the only feature visible in the OH* spectroscopic scan of the blue whirl is the vortex rim. This indicates that a significant fraction of the combustion occurs in the vortex rim, thus explaining the relatively high temperatures observed in the region immediately above the vortex rim, which most likely consists of hot gaseous products. In contrast, OH* chemiluminescence of a yellow fire whirl shows a significant difference in the location of the reaction front. The burning in a yellow fire whirl is not localized – while a significant portion burns immediately atop the fuel surface, combustion reactions continue to release heat in the swirling structure above the fuel surface. As expected, the appearance of this structure in the UV is independent of both fuel and surface types used in this study. Similar results obtained for the different fuels over the water and metal surfaces are shown in *Figures 47 and 48* in the appendix.

4.5 Surface boundary conditions for formation

As described in section *3.5*, various surface boundary conditions were studied to observe their effect on the formation of a steady blue whirl. The schematics of the different conditions are provided in *Figure 19*. *Table 4* summarizes these surface boundary conditions tested and their effect on the formation of a traditional yellow fire whirl, a transitional-blue whirl that appeared both blue and yellow (showing signs of recirculation zones), and a blue whirl with physical characteristics similar to that shown in *Table 4*. Results show that a stable blue whirl is produced in configurations (i) and (ii), but it was only briefly produced in configuration (iii). *Figure 34* shows the most stable blue whirls produced in configurations (i) – (iii). The occurrence of the blue whirl with different boundaries demonstrates that a water surface is not necessary for

the formation of a blue whirl. Configurations (iv) and (v) never produced a blue whirl. The transitional blue whirl was observed to stably exist in configuration (iii), while a weak unstable blue whirl appeared fleetingly. The blue whirl could not be sustained over the flat porous ceramic surface in any combination of fuel flow rate and entrainment gap width. A significant portion of the heptane was observed to seep through the porous surface, and it is thought that the fuel evaporation rate may not have been sufficient to generate enough swirl to sustain a blue whirl.

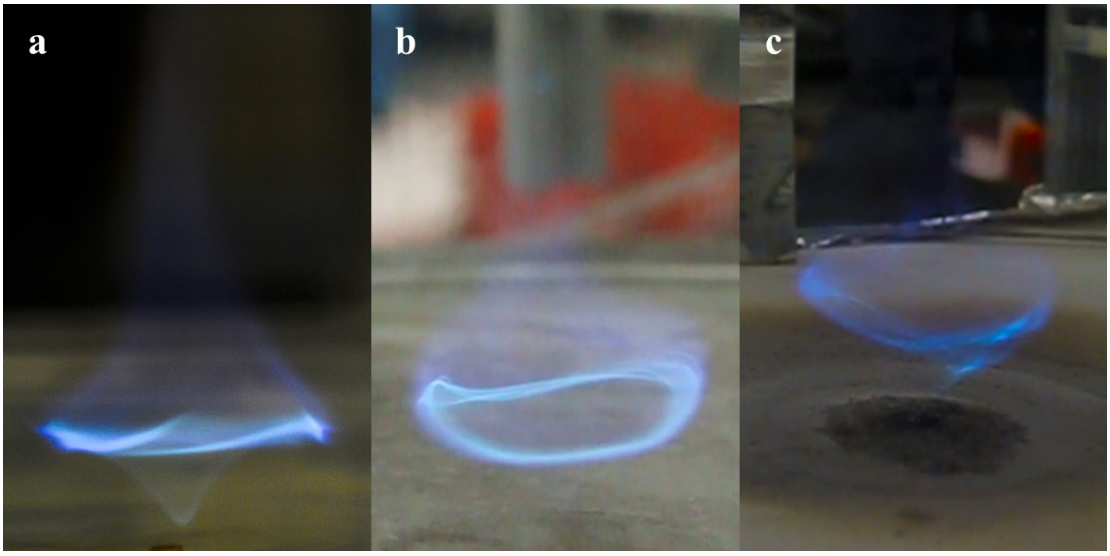

Figure 34. Blue whirls formed over a. Water surface (i); b. Steel plate (ii); c. Porous ceramic surface (iii).

Figure 35. Comparison of fire whirls formed in (a) Configuration *(iv)*; (b) Configuration *(v)*; (c) Sustained transitional-blue regime in *(iii)*.

Table 4. Summary of different surface boundary conditions tested and their effect on the formation of the blue whirl.

	Surface Boundary Condition	**Image**	**Traditional Yellow Fire Whirl**	**Transitional-Blue Whirl**	**Blue Whirl**
(i)	Water surface	Figure 34a	Yes	Yes	Yes
(ii)	Smooth stainless steel surface	Figure 34b	Yes	Yes	Yes
(iii)	Porous ceramic fibre surface	Figures 34c, 35c	Yes	Yes	Weak
(iv)	Fuel dish over the steel surface	Figure 35a	Yes	No	No
(v)	Fuel dish embedded beneath porous ceramic sheet	Figure 35b	Yes	No	No

Configurations (iii) and (iv) with a fuel dish have typically been used for generating fire whirls with liquid fuels in laboratories [2,3,12,21]. When a dish is used to contain the fuel within the enclosure, no transitional-blue or blue whirl was observed, which may be attributed to the presence of the lip, which causes a flow structure different from configurations (i) and (ii). More discussion is presented in section *5.1*. It can also be noted in *Figures 35 a and b* that the heptane burns very close to the lip on the inside of the dish, with flames rising over the lip. This suggests that the flow patterns are different as compared to a completely flat surface, even when a yellow fire whirl is formed. The may be attributed to the presence of the dish lip, and provides hints regarding the surface boundary conditions required to form a blue whirl. The presence of a fuel pan lip has been reported to stabilize pool fires and even increase

burning rate [64]. An unimpeded surface without lips or vertical obstructions appears to lead to the formation of a blue whirl.

Chapter 5: Discussion

The experiments performed in this study were designed to understand different aspects of the blue whirl. The blue whirl evolves from a traditional yellow fire whirl, and the measurements presented here bring to the fore several important distinctions. Using these results as a foundation, preliminary ideas regarding the nature and structure of the blue whirl are discussed in this chapter.

5.1 The conditions for formation

The effect of the Ekman-type boundary layer at the base of a fire whirl has been known to affect the shape of the flame near the surface [12]. *Figure 36* shows the effect of the Ekman layer on the structure of fire whirls formed using methanol. When a fuel pan is used, the air flow over the lip causes separation and re-attachment, which is thought to inhibit the formation of the blue whirl. The difference between Case B in *Figure 36* and configuration (v) discussed previously is the level of fuel present in the pan. The level of fuel in configuration (v) (depicted in *Figure 19c*) is much below the lip level, but Case B in *Figure 36* contains fuel up to the level of the lip (and thus flush with the surface over which the fire whirl is formed) which permits the formation of an Ekman-type boundary layer.

Additionally, the blue whirl is observed to have heat release over a small area, as opposed to previous configurations (gas burners, fuel soaked wicks, or pans with only fuel) that increase the fuel evaporation area, consequently leading to heat release over a larger area. The fact that a porous surface generated only a marginal and unstable

blue whirl suggests that the area over which fuel evaporation occurs plays a key role in the formation of the blue whirl. In the blue whirl regime, the vortex core (the blue cone) occupies a relatively a smaller fraction of the enclosure, as compared to the area of the vortex core in a traditional fire whirl.

Since most apparatus that have previously been used to study fire whirls in the laboratory use fuel pans with lips, or gaseous fuels with significant axial velocity, they affect the smooth inlet boundary conditions that are observed to be required for blue whirl formation, contributing to its delayed discovery. It may be possible to form the blue whirl with a gaseous fuel if the fuel could be concentrated geometrically in the radial direction, while ensuring significant axial velocity does not affect the flow field within the enclosure.

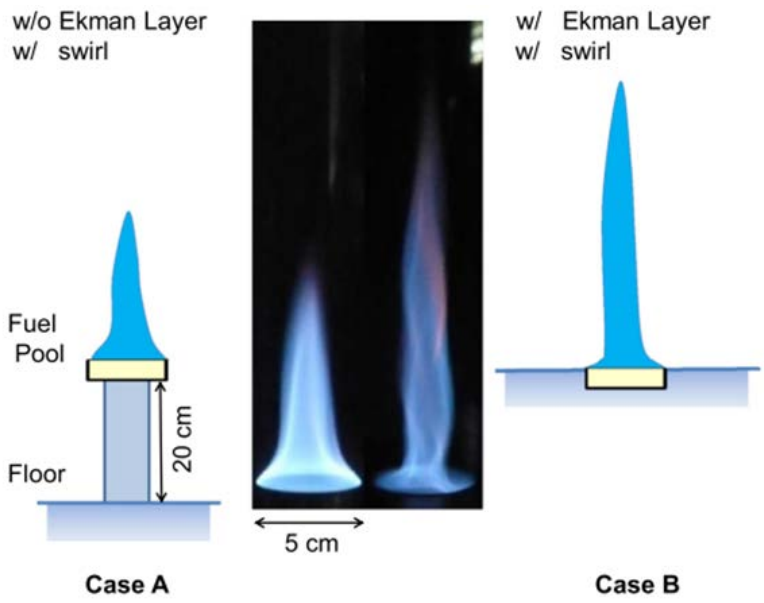

Figure 36. The effect of the formation of an Ekman-layer on the formation of a fire whirl as described in [12].

Based on the different fire whirl regimes proposed in [16], it appears that the blue whirl is close to the extinction limit supported by fast mixing of the entrained air with the evaporating fuel immediately below the flame [4]. This is similar to observations in [31] where the bubble mode was observed near the lean-blowout limit of a swirl dump combustor. In the blue whirl apparatus, the heat release could be increased by supplying more fuel than necessary to sustain the blue whirl, resulting in a transition to the conical whirl, with higher flow rates resulting in the cylindrical fire whirl. The blue whirl appears to be a stable mode, so long as significant disturbances are not introduced into the flow. Destabilization was observed when the water surface was perturbed, probes were moved within the blue cone, or air entrainment was disturbed by significant movement outside the enclosure.

It is unclear why the presence of a gap between the lower end of the quartz enclosures and the water surface affects the stability of the blue whirl, although in general, a small gap was observed to significantly sustain the existence of the blue whirl. At present, the investigation has been limited to a condition where the blue whirl evolves from a traditional yellow fire whirl. As it has been shown, the blue whirl is very sensitive to the surface conditions of the bottom boundary, and it is unclear whether the yellow whirl stage can be skipped altogether for direct formation of the blue whirl stage. Depending on the amount of fuel ignited and the vorticity already present within the enclosure prior to ignition, the period of existence of the traditional fire whirl can be shortened. Direct occurrence of the blue whirl is expected to be possible, provided the amount of fuel upon the surface and vortex strength within the

enclosure prior to ignition are close to, or at the right combination to support the formation of the blue whirl.

5.2 The Structure

This study shows that the general physical structure of the blue whirl remained independent of the surface material (*Figure 34*). Whirls were observed to be slightly wider when formed over the metal surface, which is evident in the temperature distribution of the two different cases (*Figures 29, 32 and 42*), and also depict the varying axial positions of the vortex rim with respect to the bottom surface boundary. The lower blue cone has a surprising resemblance to the under-ventilated Burke-Schumann diffusion flame [65]. A recent study [66] found that swirl (within the vortex breakdown regime) causes a change in the length of the Burke-Schumann reaction sheet. Any direct correlations to the blue whirl are as yet unclear.

The observation of recirculation zones within the blue whirl leads to the postulation that the blue whirl assumes its shape due to vortex breakdown. Specifically, the predominant axisymmetric mode of breakdown resulting in a stagnation point and recirculation zone on the swirl axis. This could explain the localized recirculating soot patterns observed using HFR imaging. The constant variation of the blue cone's size could may be explained by a combination of the following reasons. First, since the position of the bubble is only quasi-steady [27] and the bottom boundary is fixed, the only mechanism which would permit repositioning of the bubble in the axial direction is the alteration of the vortex rim location, effectively changing the size of the blue cone region. Second, the bubble mode could be a Type 1 vortex breakdown, which is

similar to Type 0, with a flattened unsteady bubble shape. In either case, fluid exchange processes (filling and emptying of the bubble) are expected to be similar to previous observations in incompressible flow by Sarpkaya [35], even in the presence of combustion induced buoyancy [30].

Figure 37. View of the blue whirl showing azimuthal soot traces, with the camera at an elevated position. Also seen is a single TFP filament glowing.

Figure 37 shows an image of the azimuthal soot trace patterns, which in conjunction with *Figure 27* reveals the three-dimensional nature of motions within the blue whirl. A schematic of the bubble filling and emptying mechanism in 2-D was presented by Escudier [67], and is represented in *Figure 38*. However, due to the three-dimensional motions observed, the nature is expected to be similar to *Figure 39*, obtained from [68] (also, *Fig. 20* in [27]). Internal flow structure within the blue whirl is not completely known yet since the flame is completely blue. The flame is observed to have a shape different from the vortex breakdown bubble, and detailed

measurements or visualization techniques will be required to confirm the analogies to previous observations of the vortex breakdown bubble.

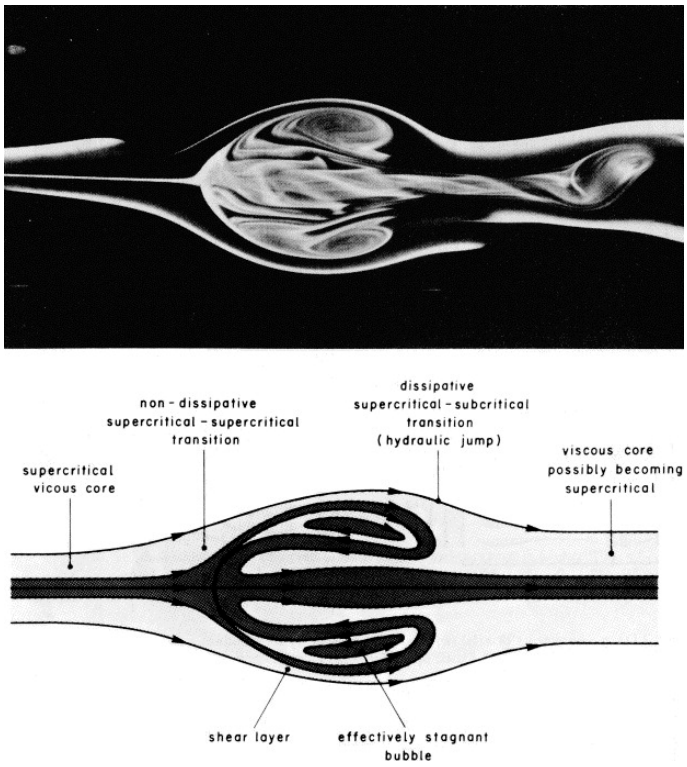

Figure 38. Schematic representation of a vortex breakdown bubble from [67].

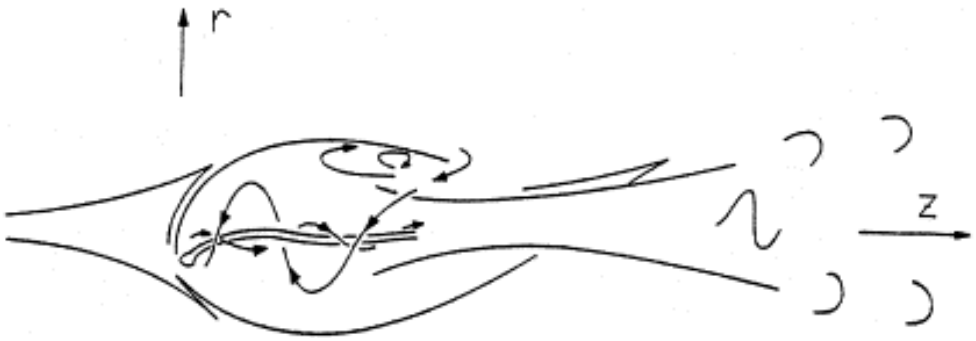

Figure 39. Schematic of 3-D flow pattern in a vortex breakdown bubble adapted from [27], and originally from [68].

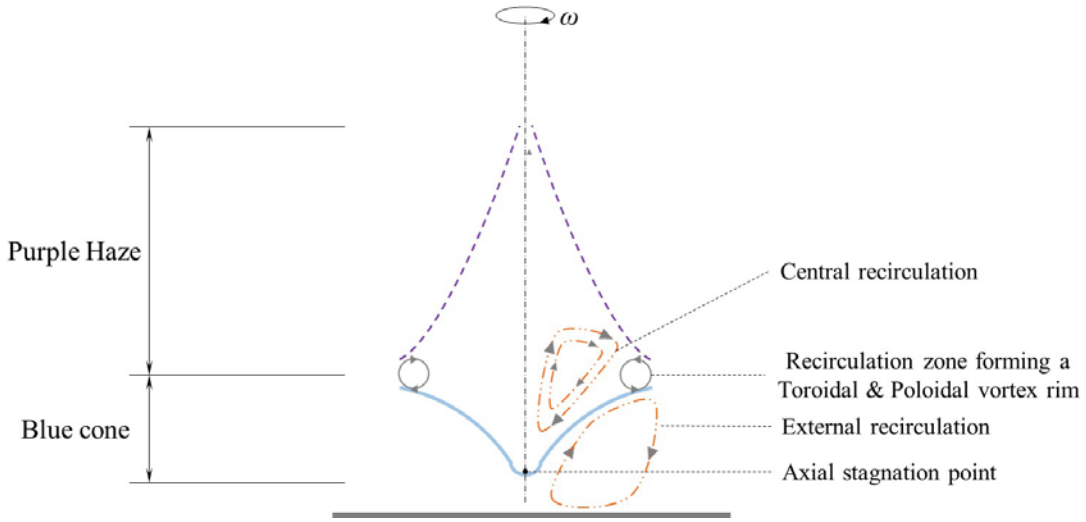

Figure 40. Proposed schematic representation of a blue whirl.

Figure 41. The famous tea-cup paradox explaining the effect of wall friction at the base (Ekman layer) on the formation of secondary flow by Einstein [69].

Based on visual observations, temperature measurements, OH* spectroscopy and vortex breakdown literature, and the idealized 2-D schematic in *Figure 38*, a schematic of the flow field of a blue whirl (a 2-D idealization) is presented in *Figure 40*, with the vortex rim analogous to the stagnant bubble recirculation zone. The region near the lower vertex of the blue cone may be similar to the axial stagnation point. Soot recirculation patterns depicted in *Figure 27* may represent the central recirculation zone. Such a flow pattern supports the general axial exit direction of the soot particles from the blue whirl. The recirculation directions depicted (in *Figure 40*) are based on

Escudier's [67] idealized pattern, and may actually be different in a reacting bubble, particularly due to the effects of buoyancy and azimuthal motions. Thus, more investigation is required to obtain detailed information on the flow patterns. The shape of the blue cone may be influenced by the Ekman layer at the base, which results in the external recirculation. This pattern is similar to the recirculation developed as a secondary flow in swirling flows, which was described by Einstein as an explanation of the tea-cup paradox (*Figure 41*) and river bank erosion [69] ([70] for English translation). The external recirculation (in *Figure 40*) should also show poloidal motion, and aid in concentrating fuel vapours and the base of the blue cone.

The three dimensional motions of soot within the blue whirl show the toroidal and poloidal motions of the vortex rim. This is to be expected, considering the whirl is seen rotating in the vortex generated within the experimental enclosure. However, the presence of these recirculating motions seems to be inherently necessary to transition from a conical fire whirl to the blue whirl.

Increased mixing as a result of these recirculation zones in the stagnant bubble (vortex rim) could explain high concentrations of OH* observed. The resulting increased reaction rates may help explain the highest temperatures being observed immediately above the vortex rim. The low soot production could have multiple explanations. Residence time effects, prevention of soot nucleation due to high strain [25] in the blue cone region are possible explanations. However, information regarding the local equivalence ratio and nature (degree of premixedness) will be required to identify the correct physical explanation. Despite many previous studies on soot formation in diffusion flames [5,25,26,71], more information about the nature of

combustion in the blue whirl is required to explain the low soot, particularly because older studies were conducted in forced counter-flow apparatus where the equivalence ratio and strain rate could be controlled. When sufficient information about the nature of combustion within the blue cone is available, similar parameters may be used in counter flow apparatus to understand the underlying phenomena better.

Soot particles are sometimes seen to escape from the vortex rim, as visible in *Figure 1b*. The soot traces used to observe fluid motions within the blue whirl are remnants from the conical whirl that are observed during a transition to the bubble mode, and their motions in an expanded central recirculation should not be confused as soot emanating from a stable blue whirl.

However, the simple schematic *Figure 40* based upon analogies with observations of vortex breakdown in non-reacting flows provides only a fluid dynamic perspective, and does not explain how the interaction of fuel and oxidizer occurs, and if premixing occurs, whether it results in a lean, rich, or stoichiometric mixture. It was suggested that there may be a layer of evaporated fuel beneath the blue cone, leading to a premixed region [4], providing another potential explanation for soot-free combustion. Previous observations of fast mixing and fluid dynamics around the flame resulted in reduced soot-precursors and led to faster destruction of soot formed in the fuel-rich regions by drawing them faster to the flame [25,26,71]. This led to the proposition by Xiao et al. [4] that similar processes occurred in the recirculating regions of the blue whirl, and may provide an explanation for the structure of the lower blue cone, rather than the vortex rim. Identifying the dominating process is critical in

identifying the right explanation for the low soot production, and a more controlled setup to investigate this deeper.

The thermal structure investigated in this study is intended to form the basis of explaining the combustion characteristics of the blue whirl. The thermal structure reveals that of the three distinct regions, the purple haze is the hottest. Based on the brightness of the vortex rim and the OH* spectroscopy results, it is expected that the vortex rim also burns at very high temperatures. However, it was observed during experiments that the blue whirl adjusted itself such that the vortex rim was usually just below the filament at 1 cm above the water (or metal) surface. Thus, temperatures of the vortex rim are not directly available through the diagnostics performed here due to the axial spatial resolution of filaments (how closely spaced the filaments are in the axial direction), but the region immediately around the vortex rim is distinctly discernible in the contours presented earlier. The lower blue cone is the coolest, observed to release heat in a thin flame sheet, which may be energy release as a result of fuel pyrolysis. A large fraction of the combustion and heat release seems to occur within the vortex rim and purple haze region, which, as evidenced by OH* spectroscopy results, which may signify an oxidation of CO to CO_2 in this region.

5.3 Importance of the traditional fire whirl and blue whirl stability

In all the experiments performed in this study, the traditional yellow fire whirl was seen to always precede the occurrence of the blue whirl. After the traditional yellow fire whirl (*Figure 1c*), two different versions of the conical fire whirl (*Figure 21*) have also been observed. These were eventually followed by the blue whirl in all

experiments. Although the relative time period of each varied depending on the level of swirl at the time of fuel ignition, all three stages were observed in the same chronological order even when destabilizations of the blue whirl occurred. This behaviour is consistent with the evolutionary pattern of vortex breakdown modes [35,37].

Vortex breakdown structures are known to exhibit positional instability, with unpredictable wander about the axis even under steady external conditions [38]. This is similar to the conical fire whirl and blue whirl showing significant wander within the enclosure. Formation of the fire whirl was accompanied by aural indications that suggested that the yellow fire whirl was turbulent in nature [4], and is similar to previous observations in fire whirls [16]. It was possible to sustain the flame in the laminar fire whirl regime (*Figure 21b*) by supplying fuel at a higher rate than required to sustain the blue whirl. The laminar state was primarily observed when the blue whirl was destabilized either due to velocity variations in the surroundings, or due to higher fuel flow rates causing an accumulation of fuel over the water surface.

In general, the stability of the blue whirl was observed to be higher with fuels that had a lower rate of evaporation. The difference in viscosity of these fuels may have also played a role in determining the area over which the fuel spread. In this study, blue whirls formed using iso-octane and cyclohexane were observed to be the most stable, while those formed using acetone and ethanol remained in the blue whirl stage for shorter periods of time and showed more instances of destabilization and reversion to the either the transitional whirl or the traditional fire whirl. With repeated tests, small amounts of combustion products were observed to accumulate over both the water and

metal surfaces. The accumulation of these viscous products was found to affect the swirling of the water surface, and at times produce blue whirls that were more stable and less prone to destabilizations. However, without a detailed and methodical analysis by varying the swirl of the water surface itself, it is difficult to make any conclusive statements about its effect on the stability of the blue whirl. To that end, a definition of blue whirl stability and criteria may need to be established to be able to make quantitative comparisons – these metrics could be based on the time of continuous existence, or even magnitude of precession around the geometric centre of the apparatus.

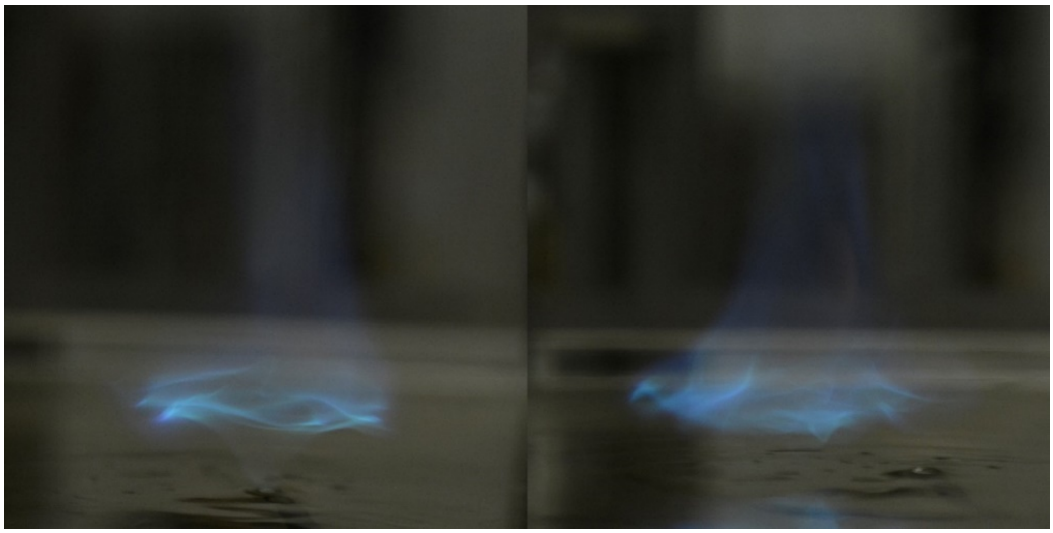

Figure 42. Vortex rim of the blue whirl showing instabilities.

The blue whirl was also observed to sometimes show instabilities in the vortex rim during initial formation from the conical fire whirl. The occurrence of these instabilities could also be induced by slightly blowing air into the enclosure through one of the slits. *Figure 42* shows such a stage captured in the space of ~3.67 s. The surface of the water immediately below the whirl can be observed to be in complete

focus, and the nature of images depicted are not due to out-of-focus blurry capture. Slight blowing into the enclosure could also be used to induce a transition from the conical fire whirl to the blue whirl, which is expected since increasing the circulation in a water-in-tube vortex breakdown setup caused the transition from a spiral mode to a bubble mode of vortex breakdown [37].

5.4 Other considerations and questions

Observations of flow downstream of the vortex breakdown bubble (Type 0) have revealed a spiral mode (Type 2) [27,29,35]. If a similar behaviour is expected with the blue whirl, the nature of flow downstream of the whirl may also show signs of the spiral breakdown. However, since soot visualization is possible only for a short axial distance beyond the vortex rim, whether such a disturbance occurs is still unclear. However, based on the sinusoidal wave-like motion patterns formed by the soot traces while exiting the purple haze (*Figure 27*), the second disturbance occurring downstream of the vortex rim could be of a double helix (Type 5) disturbance originally identified by Sarpkaya [35]. Further investigations to identify the nature of fluid motion downstream of the blue whirl will provide more insight into the actual structure of a second disturbance, if it exists.

Although the general structure may be explained on the basis of vortex breakdown, the cause for the non-sooting nature and precise modes of combustion still need further investigation. Whether the fluid dynamics prevent soot formation, or if the combustion occurring is in a regime that is less prone to soot formation (for example, lean premixed etc.) is still unclear. The coupling of the fluid dynamics and chemistry

which affects the location of combustion, and the mixing and interaction of air and fuel vapours are still open questions.

5.5 Potential applications

Since the blue whirl has been observed to occur even when burning crude oil [4], this presents opportunities to design stationary burners that may be of use in rural settings where the use of coal or wood fired stoves are predominant. In this scenario, the benefits of soot free combustion are more attractive than energy efficiency gains. The simple setup required could assure high affordability and minimal maintenance. Flame-holding capabilities of a reacting vortex breakdown bubble was predicted by Faler [36], and provide opportunities for implementation in continuous air-breathing engines such as gas turbines. Designing an apparatus for steady observation of the regime will be critical, and could be based on previous designs of whirl [6,40] or swirl combustion [31].

Chapter 6: Conclusion

The blue whirl is a newly discovered flame structure that evolves naturally from a traditional yellow fire whirl in a fixed-frame self-entraining setup. The defining characteristic is the absence of soot in the flame, even when directly burning a sooty liquid hydrocarbon. Original discovery of the flame was made while studying the formation of fire whirls over a water surface. The physical structure observed is comprised of three distinct regions – a lower blue cone, a bright ring (the vortex rim), and a purple haze above. Although initial discovery was made while studying the formation of fire whirls over a water surface, it has been shown that the blue whirl can be produced over any smooth and unimpeded surface, indicating that its formation is governed primarily by the flow structure over the incoming boundary layer.

The temperature distribution of the whirl was investigated using micro-thermocouples and thin-filament pyrometry. The temperatures obtained through these diagnostics reveal that the flame burns hotter than expected for a diffusion flame, with temperatures in the purple haze peaking around ~2000 K. Most of the combustion was observed to occur in the thin vortex rim region through OH* spectroscopy. In contrast, the yellow whirl was observed to burn relatively continuously from the fuel surface and in the whirling flames above.

The blue whirl regime has been shown to form over a variety of liquid hydrocarbon fuels with a similar thermal structure that it is not qualitatively altered by the bottom surface boundary over which the whirl is formed. Thus, it is postulated that a combination of the heat release rate and the resulting buoyancy, the circulation

present within the setup and the resulting vortex breakdown, together affect the formation of the blue whirl, rather than the composition of the fuel itself.

Many open questions still remain. Utilization of the phenomenon in an engineering application will not be evident until the processes governing the formation are understood better, but the blue whirl regime does appear attractive due to low soot emissions. Measurements presented here provide a basis for developing a theory by highlighting the important role the vortex ring plays in the combustion process. Further investigations will be necessary to identify the nature of combustion within the blue whirl (degree of premixedness; local equivalence ratios). The exact combination of circulation strength and heat release rate that will produce the blue whirl still remains to be established. It also remains to be seen whether such a regime can be observed with gaseous fuels, but it is expected to be possible since the regime appears to be governed by the fluid dynamics around the flame rather than the composition of the fuel.

Although fire whirls have been studied in considerable detail previously, primarily due to their destructive nature when they form in urban or wildland fires, investigations of their utility in efficient energy generation has been minimal, and the blue whirl has the potential to contribute toward this purpose. Many applications are possible considering liquid fuels may be used directly; stationary burners and other low Mach combustion devices may be appropriate for implementation.

6.1 Opportunities for Future Work

The relatively recent discovery of this flame regime provides ample opportunities for future study. First, the development of the blue whirl in other traditional fire whirl apparatus may be investigated. Since primary factors such as the fuel flow and resulting heat release, and the velocity and resulting circulation are strongly linked, it would be instructive to design an apparatus that allows for independent and decoupled control over each parameter to study the magnitude of each of these effects. Such an apparatus would provide an opportunity to develop a "map" relating the circulation within the enclosure and the buoyancy, and the range of values within which the blue whirl may form can be ascertained; this map could also provide interesting information regarding dimensional scaling of the blue whirl. In addition, reducing excessive flame wander, while allowing sufficient access for physical probing and optical diagnostics would be helpful in reducing experimental errors.

The occurrence of the blue whirl in other vortex breakdown systems that don't require a bottom surface boundary could show potential in engineering applications. This could be done by inducing vortex breakdown in a traditional pipe configuration, and then injecting gaseous fuels to identify if the flame evolution is similar.

OH* chemiluminescence of the blue whirl presented here is only a qualitative analysis to identify the reaction front. A more detailed study involving different species and their relative concentration ratios may help in identifying regions of the flame that may be rich, lean or stoichiometric; premixed, diffusion or partially premixed. Finally, velocity measurements can provide important information regarding the vortex structure within the flame and in the free vortex around it. This could also provide

details on the mixing mechanisms of air and fuel, which can help predicting whether the equivalence ratios within the flame.

When sufficient experimental information about the blue whirl regime is available, macroscopic results, including the ones presented here could be used to validate numerical simulations, which will be crucial to understand the micro-scale processes. Such a simulation could also highlight the dominating mechanisms, and thus provide insight into methods of establishing control over its formation. This would then provide sufficient understanding to design a practical combustion device.

Appendix

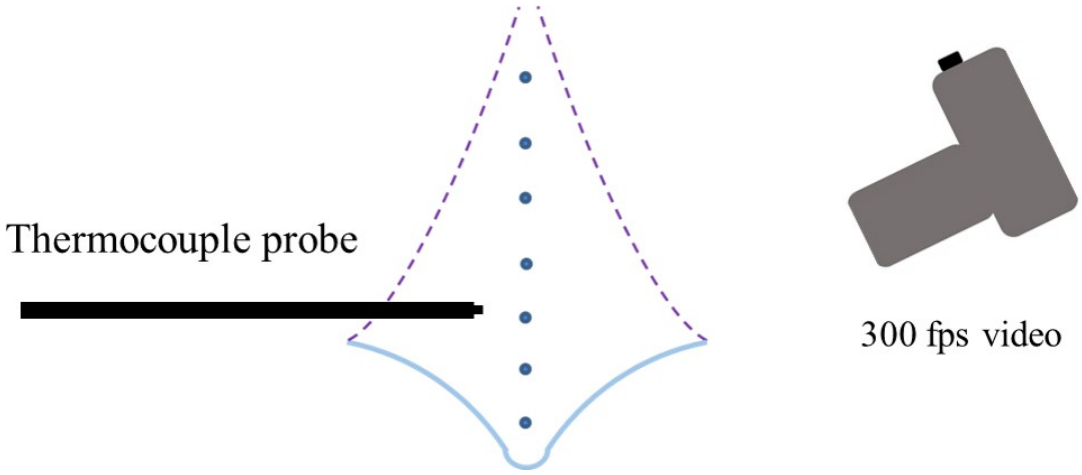

Figure 43. Schematic of thermocouple measurements performed on the blue whirl.

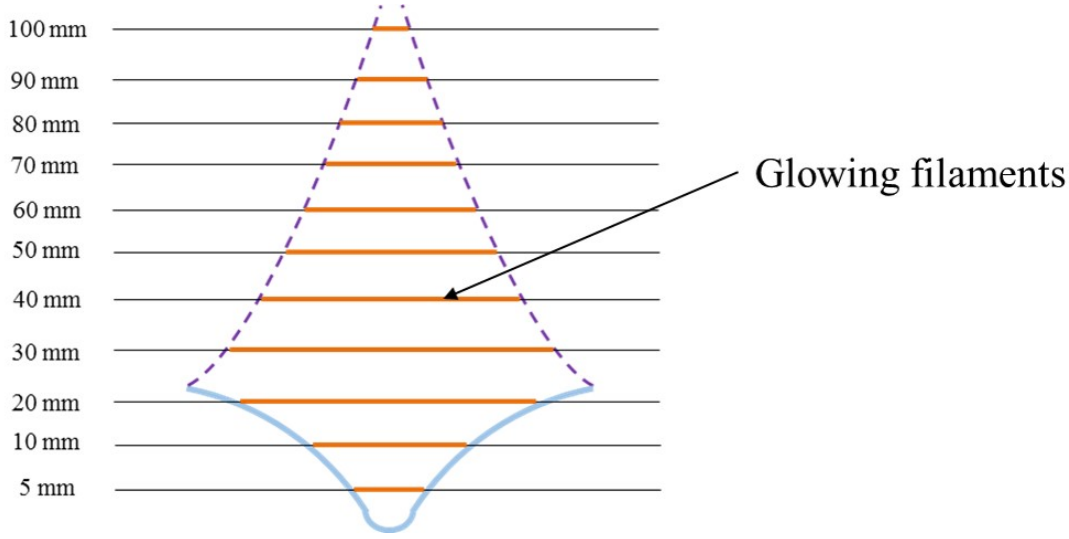

Figure 44. Schematic of blue whirl interaction with SiC filament array.

(Relative height of blue whirl only for representation. Height of blue whirl, and consequently, the number of filaments within blue cone region changes continuously.)

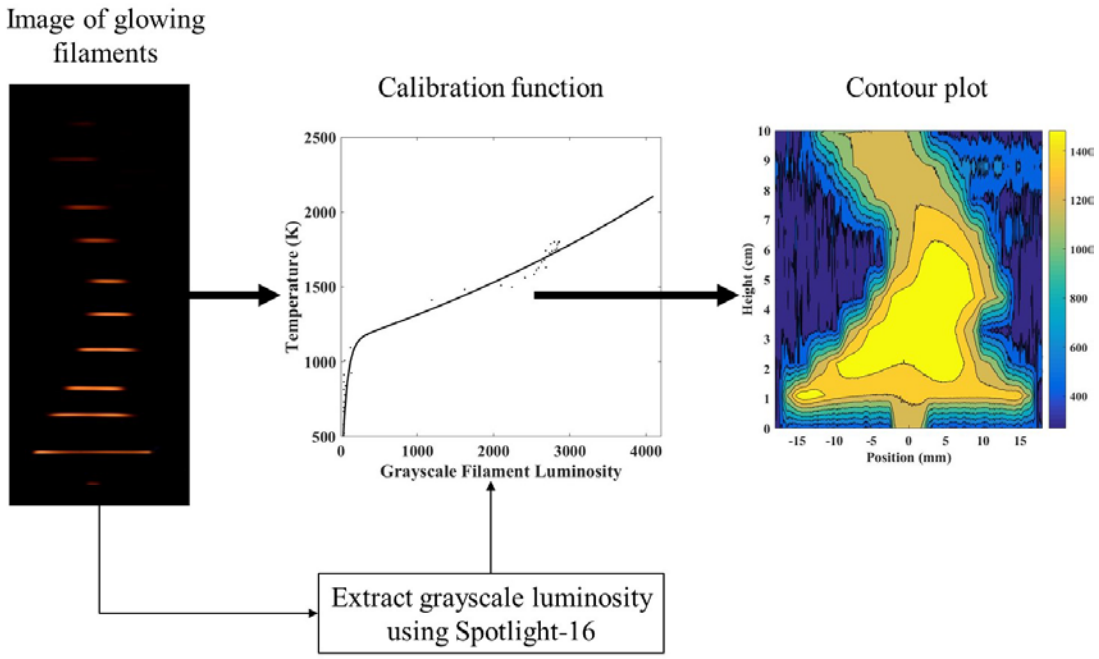

Figure 45. General procedure for performing thin-filament pyrometry for temperature measurements.

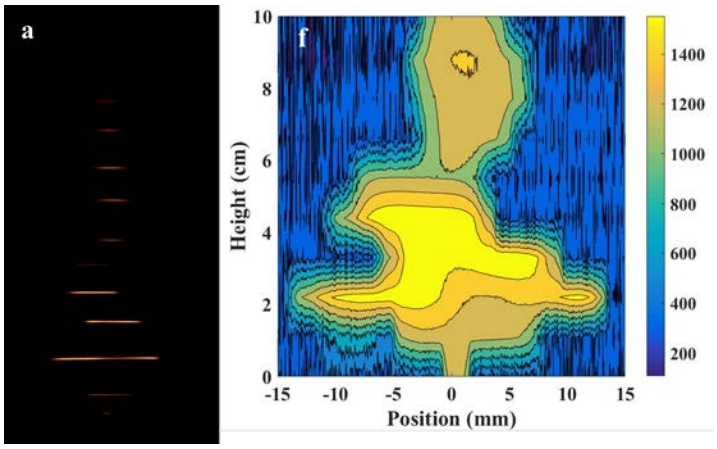

Figures 46 a, f

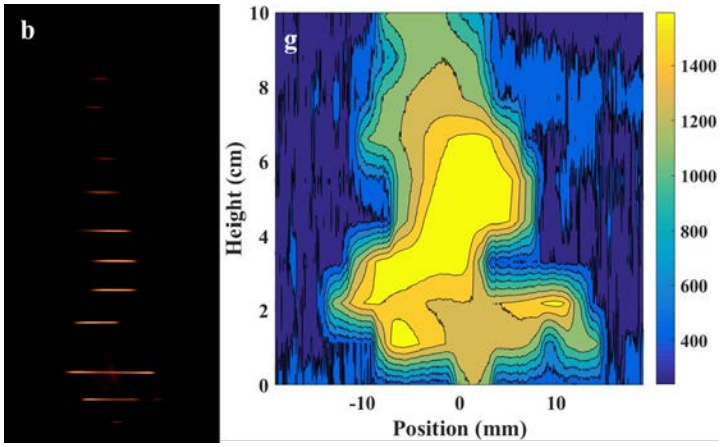

Figures 46 b, g

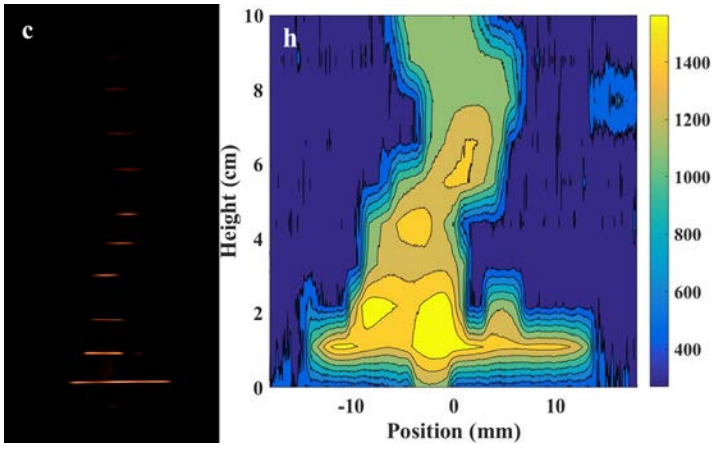

Figures 46 c, h

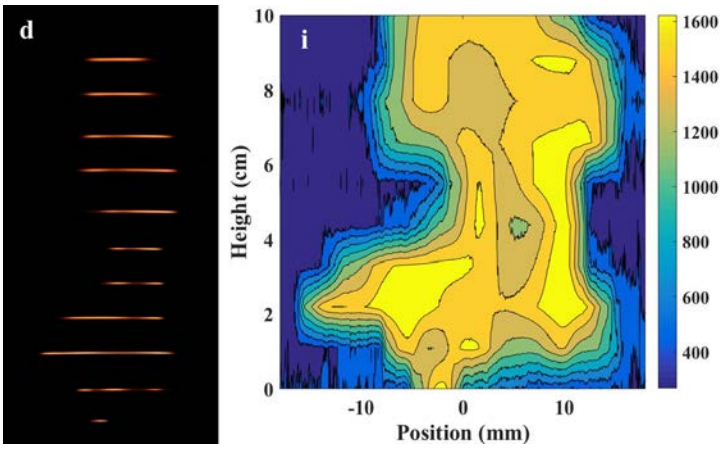

Figures 46 d, i

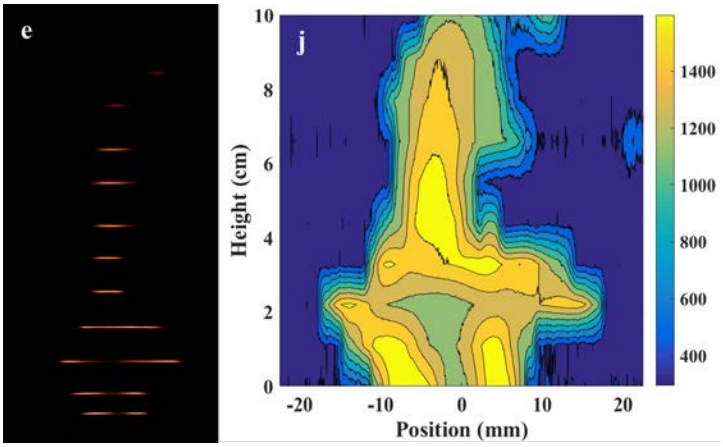

Figures 46 e, j

Figure 46. Instantaneous TFP images of filaments and correponding temperature contours of blue whirls formed over a metal surface using (a, f) heptane, (b, g) iso-octane, (c, h) cyclohexane, (d, i) acetone, and (e, j) ethanol.

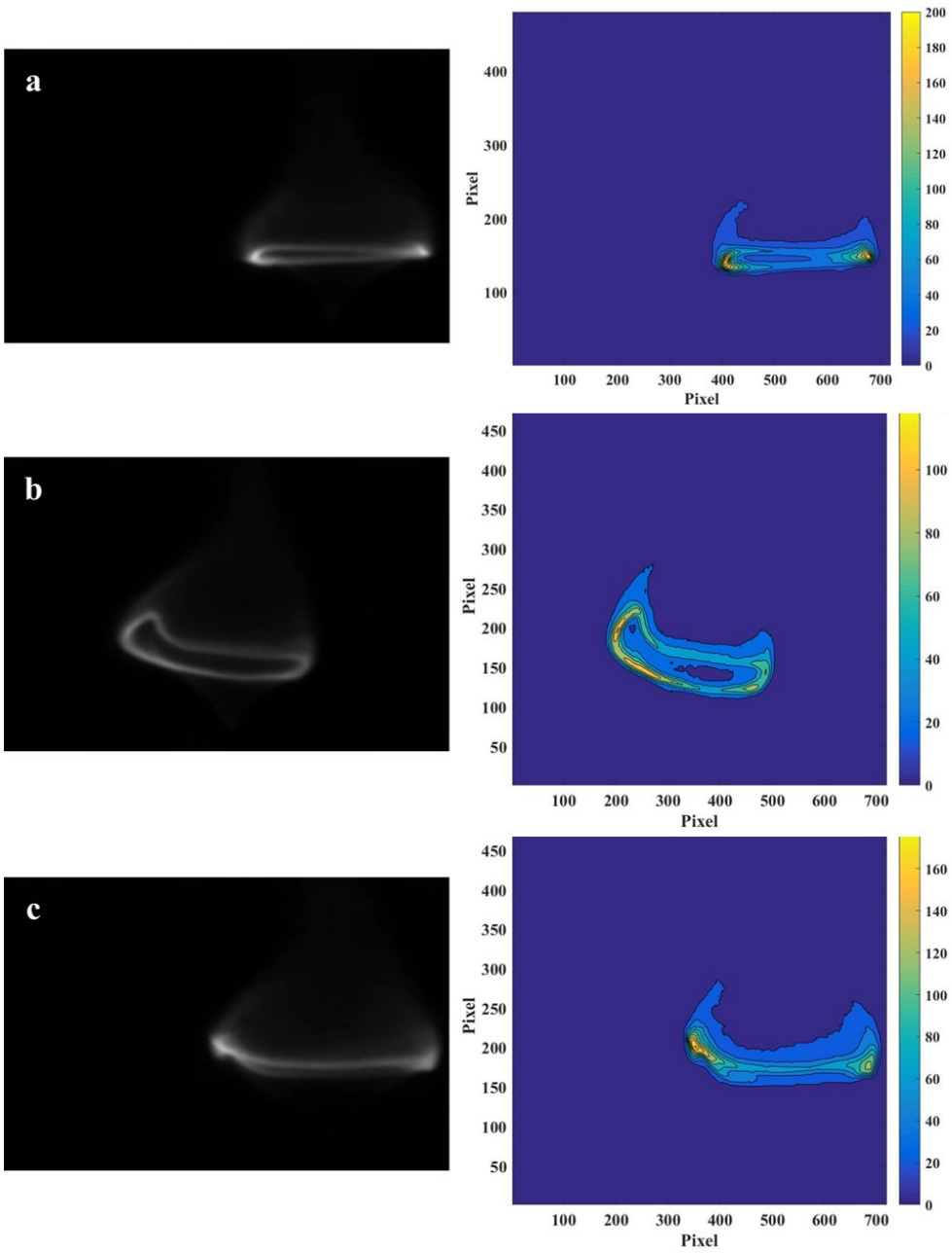

Figure 47. OH* chemiluminescence of blue whirls formed over water surface using (a) heptane, (b) iso-octane, and (c) cyclohexane.

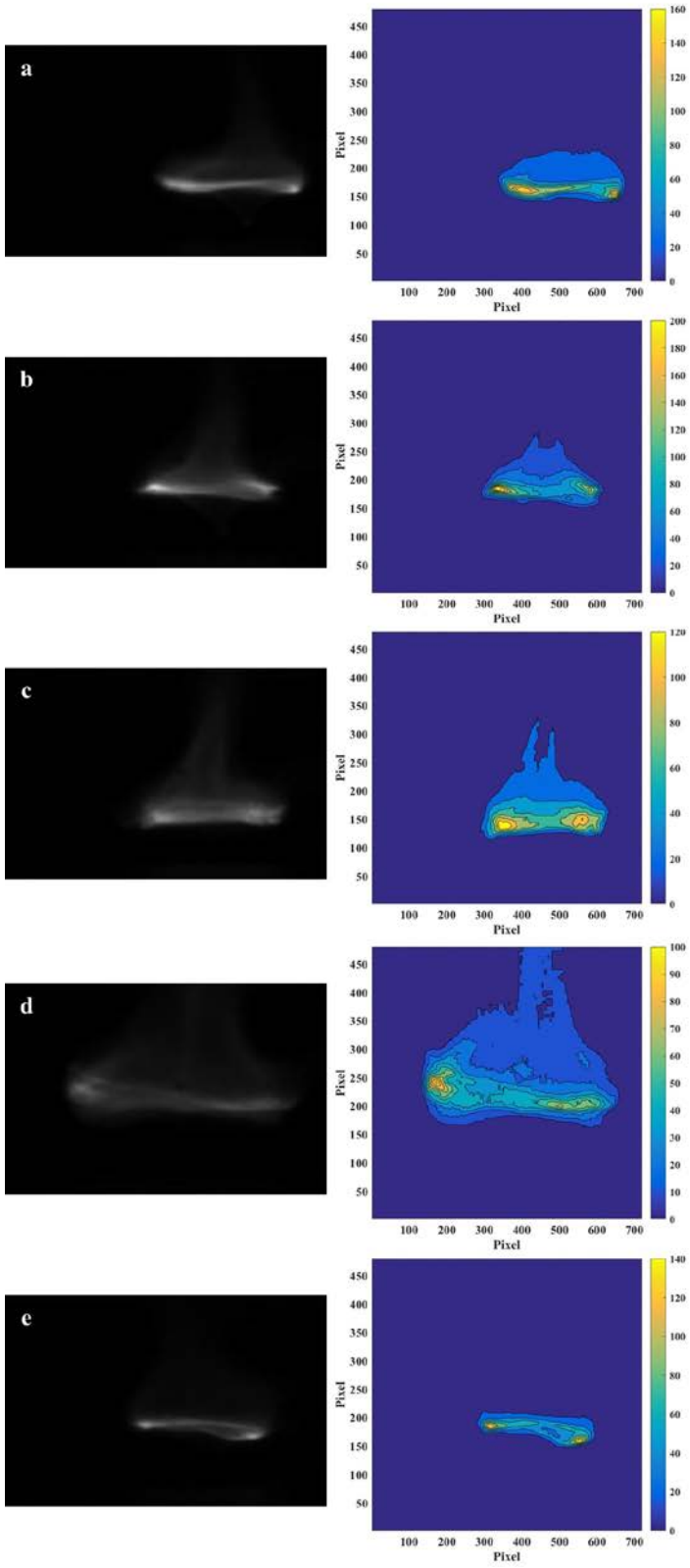

Figure 48. OH* chemiluminescence of blue whirls formed over flat metal plate using (a) heptane, (b) iso-octane, (c) cyclohexane, (d) acetone, and (e) ethanol.

References

[1] G.E. Byram, R.E. Martin, Fire Whirlwinds in the Laboratory, Fire Control Notes. 23 (1962) 13–17. https://www.frames.gov/catalog/11826.

[2] G.M. Byram, R.E. Martin, The Modeling of Fire Whirlwinds, For. Sci. 16 (1970) 386–399. http://www.ingentaconnect.com/content/saf/fs/1970/00000016/00000004/art00003.

[3] H.W. Emmons, S.-J. Ying, The fire whirl, Symp. Combust. 11 (1967) 475–488. doi:10.1016/S0082-0784(67)80172-3.

[4] H. Xiao, M.J. Gollner, E.S. Oran, From fire whirls to blue whirls and combustion with reduced pollution, Proc. Natl. Acad. Sci. 113 (2016) 9457–9462. doi:10.1073/pnas.1605860113.

[5] K.-C. Lin, G.M. Faeth, State Relationships of Laminar Permanently-Blue Opposed-Jet Hydrocarbon-Fueled Diffusion Flames, Int. J. Environ. Combust. Tech. Vol I. (2000) 53–79.

[6] R.A. Yetter, I. Glassman, H.C. Gabler, Asymmetric Whirl Combustion: A New Low NOx Approach, Proc. Combust. Inst. 28 (2000) 1265–1272. doi:10.1016/S0082-0784(00)80339-2.

[7] A. Tohidi, M.J. Gollner, H. Xiao, Fire whirls, Annu. Rev. Fluid Mech. 50 (2018). doi:10.1146/annurev-fluid-122316-045209.

[8] M.I. Hassan, K. Kuwana, K. Saito, F. Wang, Flow structure of a fixed-frame type fire whirl, Fire Saf. Sci. (2005) 951–962. doi:10.3801/IAFSS.FSS.8-951.

[9] K.A. Hartl, A.J. Smits, Scaling of a small scale burner fire whirl, Combust. Flame. 163 (2016) 202–208. doi:10.1016/j.combustflame.2015.09.027.

[10] P. Wang, N. Liu, L. Zhang, Y. Bai, K. Satoh, Fire Whirl Experimental Facility with No Enclosure of Solid Walls: Design and Validation, Fire Technol. 51 (2015) 951–969. doi:10.1007/s10694-014-0435-0.

[11] K. Zhou, N. Liu, J.S. Lozano, Y. Shan, B. Yao, K. Satoh, Effect of flow circulation on combustion dynamics of fire whirl, Proc. Combust. Inst. 34 (2013) 2617–2624. doi:10.1016/j.proci.2012.06.053.

[12] R. Dobashi, T. Okura, R. Nagaoka, Y. Hayashi, T. Mogi, Experimental Study on Flame Height and Radiant Heat of Fire Whirls, Fire Technol. 52 (2016) 1069–1080. doi:10.1007/s10694-015-0549-z.

[13] J. Lei, N. Liu, L. Zhang, H. Chen, L. Shu, P. Chen, Z. Deng, J. Zhu, K. Satoh, J.L. De Ris, Experimental research on combustion dynamics of medium-scale fire whirl, Proc. Combust. Inst. 33 (2011) 2407–2415. doi:10.1016/j.proci.2010.06.009.

[14] P. Wang, N. Liu, K. Hartl, A. Smits, Measurement of the Flow Field of Fire Whirl, Fire Technol. 52 (2016) 263–272. doi:10.1007/s10694-015-0511-0.

[15] J. Lei, N. Liu, Reciprocal transitions between buoyant diffusion flame and fire whirl, Combust. Flame. 167 (2016) 463–471. doi:10.1016/j.combustflame.2015.10.009.

[16] J. Lei, N. Liu, Y. Jiao, S. Zhang, Experimental investigation on flame patterns

of buoyant diffusion flame in a large range of imposed circulations, Proc. Combust. Inst. 36 (2016) 3149–3156. doi:http://dx.doi.org/10.1016/j.proci.2016.06.072.
[17] J. Lei, N. Liu, L. Zhang, K. Satoh, Temperature, velocity and air entrainment of fire whirl plume: A comprehensive experimental investigation, Combust. Flame. 162 (2015) 745–758. doi:10.1016/j.combustflame.2014.08.017.
[18] K. Satoh, N. Liu, Q. Liu, K.T. Yang, Numerical and Experimental Study of Merging Fires in Square Arrays, ASME 2007 Int. Mech. Eng. Congr. Expo. 8 (2007) 461–472. doi:10.1115/IMECE2007-43220.
[19] J.M. Forthofer, S.L. Goodrick, Review of vortices in wildland fire, J. Combust. 2011 (2011). doi:10.1155/2011/984363.
[20] J. Lei, N. Liu, K. Satoh, Buoyant pool fires under imposed circulations before the formation of fire whirls, Proc. Combust. Inst. 35 (2015) 2503–2510. doi:10.1016/j.proci.2014.05.110.
[21] K.H. Chuah, G. Kushida, The prediction of flame heights and flame shapes of small fire whirls, Proc. Combust. Inst. 31 II (2007) 2599–2606. doi:10.1016/j.proci.2006.07.109.
[22] K. Kuwana, S. Morishita, R. Dobashi, K.H. Chuah, K. Saito, The burning rate's effect on the flame length of weak fire whirls, Proc. Combust. Inst. 33 (2011) 2425–2432. doi:10.1016/j.proci.2010.05.049.
[23] Y. Hayashi, K. Kuwana, R. Dobashi, Influence of Vortex Structure on Fire Whirl Behaviour, Fire Saf. Sci. 10 (2011) 459–470. doi:10.3801/IAF.
[24] A.Y. Klimenko, F.A. Williams, On the flame length in firewhirls with strong vorticity, Combust. Flame. 160 (2013) 335–359. doi:10.1016/j.combustflame.2012.10.019.
[25] K.-C. Lin, G.M. Faeth, Hydrodynamic suppression of soot emissions in laminar diffusion flames, J. Propuls. Power. 12 (1996) 10–17. doi:10.2514/3.23984.
[26] K.C. Lin, G.M. Faeth, Effects of hydrodynamics on soot formation in laminar opposed-jet diffusion flames, J. Propuls. Power. 12 (1996) 691–698. doi:10.2514/3.24090.
[27] O. Lucca-Negro, T. O'Doherty, Vortex breakdown: A review, Prog. Energy Combust. Sci. 27 (2001) 431–481. doi:10.1016/S0360-1285(00)00022-8.
[28] S. Leibovich, The Structure of Vortex Breakdown, Annu. Rev. Fluid Mech. 10 (1978) 221–246. doi:10.1146/annurev.fl.10.010178.001253.
[29] J.K. Harvey, Some observations of the vortex breakdown phenomenon, J. Fluid Mech. 14 (1962) 585. doi:10.1017/S0022112062001470.
[30] N. Syred, J.M. Beér, Combustion in swirling flows: A review, Combust. Flame. 23 (1974) 143–201. doi:10.1016/0010-2180(74)90057-1.
[31] M. Thiruchengode, Sensing and Dynamics of Lean Blowout in a Swirl Dump Combustor, 2006.
[32] M.R. Ruith, P. Chen, E. Meiburg, T. Maxworthy, Three-dimensional vortex breakdown in swirling jets and wakes: direct numerical simulation, J. Fluid Mech. 486 (2003) 331–378. doi:10.1017/S0022112003004749.
[33] M.S. Broadhurst, Vortex Stability and Breakdown : Direct Numerical Simulation and Stability Analysis using BiGlobal and Parabolised

Formulations, Thesis Imp. Coll. London. (2006).
[34] C. Brucker, Study of vortex breakdown by particle tracking velocimetry (PTV) Part 2: Spiral-type vortex breakdown, Exp. Fluids. 139 (1993) 133–139.
[35] T. Sarpkaya, On stationary and travelling vortex breakdowns, J. Fluid Mech. 45 (1971) 545. doi:10.1017/S0022112071000181.
[36] J.H. Faler, Some Experiments in Swirling Flows: Detailed Velocity Measurements of a Vortex Breakdown using a Laser Doppler Anemometer, Cornell University, 1976. https://ntrs.nasa.gov/search.jsp?R=19770008055.
[37] J.H. Faler, S. Leibovich, Disrupted states of vortex flow and vortex breakdown, Phys. Fluids. 20 (1977) 1385. doi:10.1063/1.862033.
[38] J.H. Faler, S. Leibovich, An experimental map of the internal structure of a vortex breakdown, J. Fluid Mech. 86 (1978) 313–335. doi:10.1017/S0022112078001159.
[39] C. Brücker, Study of vortex breakdown by particle tracking velocimetry (PTV): Part 1: Bubble-type vortex breakdown, Exp. Fluids Exp. Methods Their Appl. to Fluid Flow. 14 (1993) 133–139. doi:10.1007/BF00196996.
[40] H.C. Gabler, R.A. Yetter, I. Glassman, Asymmetric Whirl Combustion : A New Approach for Non-Premixed Low NOx Gas Turbine Combustor Design, (1998) 1–11.
[41] J. Buckmaster, Edge-flames, Prog. Energy Combust. Sci. 28 (2002) 435–475. doi:10.1016/S0360-1285(02)00008-4.
[42] Thermocouple Tolerances Tolerance Value Tolerance Value Tolerance Value, Omega Thermocouples. (n.d.) 1–7. http://www.omega.com/techref/colorcodes.html.
[43] A. V. Singh, M.J. Gollner, A methodology for estimation of local heat fluxes in steady laminar boundary layer diffusion flames, Combust. Flame. 162 (2015) 2214–2230. doi:10.1016/j.combustflame.2015.01.019.
[44] V. Vilimpoc, L.P. Goss, B. Sarka, Spatial temperature-profile measurements by the thin-filament-pyrometry technique, 13 (1988) 93–95.
[45] V. Vilimpoc, L.P. Goss, SiC-Based thin-filament pyrometry: Theory and thermal properties, Symp. Combust. 22 (1989) 1907–1914. doi:10.1016/S0082-0784(89)80205-X.
[46] S. Pauzin, A. Giovannini, B. Bédat, Thin filament infrared pyrometry: instantaneous temperature profile measurements in a weakly turbulent hydrocarbon premixed flame, Exp. Fluids. 17 (1994) 397–404. doi:10.1007/BF01877042.
[47] W.M. Pitts, Thin-filament pyrometry in flickering laminar diffusion flames, Symp. Combust. 26 (1996) 1171–1179. doi:10.1016/S0082-0784(96)80333-X.
[48] G. Wang, C. Bonilla, D. Kalitan, Gas Temperature Field Measurement using Thin-Filament Pyrometry, in: Proc. ASME Turbo Expo Turbine Tech. Conf. Expo. GT2014, Dusseldorf, Germany, 2014: pp. 1–11. doi:10.1115/GT2014-25909.
[49] H. Guo, J. a. Castillo, P.B. Sunderland, Digital camera measurements of soot temperature and soot volume fraction in axisymmetric flames, Appl. Opt. 52 (2013) 8040–8047. doi:10.1364/AO.52.008040.
[50] J. D. Maun, Thin filament pyrometry with a Digital Still Camera - MS Thesis,

University of Maryland, 2006. http://drum.lib.umd.edu/handle/1903/3602.
[51] J.D. Maun, P.B. Sunderland, D.L. Urban, Thin-filament pyrometry with a digital still camera., Appl. Opt. 46 (2007) 483–488. doi:10.1364/AO.46.000483.
[52] R.S. Klimek, R. B., Wright, T. W., Sielken, Color Image Processing Tracking System and Object, NASA Tech. Memo. 1017144 (NASA Lewis Res. Cener). (1996). https://ntrs.nasa.gov/search.jsp?R=19960016954.
[53] Y.K. Jeong, C.H. Jeon, Y.J. Chang, Evaluation of the equivalence ratio of the reacting mixture using intensity ratio of chemiluminescence in laminar partially premixed CH4-air flames, Exp. Therm. Fluid Sci. 30 (2006) 663–673. doi:10.1016/j.expthermflusci.2006.01.005.
[54] M. Orain, Y. Hardalupas, Effect of fuel type on equivalence ratio measurements using chemiluminescence in premixed flames, Comptes Rendus Mécanique. 338 (2010) 241–254. doi:10.1016/j.crme.2010.05.002.
[55] Y. Hardalupas, M. Orain, Local measurements of the time-dependent heat release rate and equivalence ratio using chemiluminescent emission from a flame, Combust. Flame. 139 (2004) 188–207. doi:10.1016/j.combustflame.2004.08.003.
[56] T.M. Muruganandam, B. Kim, R. Olsen, M. Patel, B. Romig, J.M. Seitzman, Chemiluminescence based sensors for turbine engines, AIAA Pap. (2003). http://www.aric.or.kr/treatise/journal/content.asp?idx=52744%5Cnhttp://arc.aiaa.org/doi/pdf/10.2514/6.2003-4490.
[57] T.M. Muruganandam, B.H. Kim, M.R. Morrell, V. Nori, M. Patel, B.W. Romig, J.M. Seitzman, Optical equivalence ratio sensors for gas turbine combustors, Proc. Combust. Inst. 30 (2005) 1601–1608. doi:10.1016/j.proci.2004.08.247.
[58] V.N. Nori, J.M. Scitzman, CH* chemiluminescence modeling for combustion diagnostics, Proc. Combust. Inst. 32 I (2009) 895–903. doi:10.1016/j.proci.2008.05.050.
[59] V. Nori, J. Seitzman, Evaluation of Chemiluminescence as a Combustion Diagnostic under Varying Operating Conditions, 46th AIAA Aerosp. Sci. Meet. Exhib. (2008) 1–14. doi:10.2514/6.2008-953.
[60] C.S. Panoutsos, Y. Hardalupas, A.M.K.P. Taylor, Numerical evaluation of equivalence ratio measurement using OH* and CH* chemiluminescence in premixed and non-premixed methane-air flames, Combust. Flame. 156 (2009) 273–291. doi:10.1016/j.combustflame.2008.11.008.
[61] I. Glassman, R.A. Yetter, Combustion, Academic Press, 2008. http://www.sciencedirect.com/science/book/9780120885732 (accessed March 25, 2017).
[62] G.H. Dieke, H.M. Crosswhite, The ultraviolet bands of OH Fundamental data, J. Quant. Spectrosc. Radiat. Transf. 2 (1962) 97–199. doi:http://dx.doi.org/10.1016/0022-4073(62)90061-4.
[63] R. Seiser, L. Truett, D. Trees, K. Seshadri, Structure and extinction of non-premixed n-heptane flames, Symp. Combust. 27 (1998) 649–657. doi:10.1016/S0082-0784(98)80457-8.
[64] A. Bouhafid, J.P. Vantelon, P. Joulain, A.C. Fernandez-Pello, On the Flame

Structure at the Base of a Pool Fire, Symp. Combust. 22 (1988) 1291–1298. doi:10.1016/S0082-0784(89)80140-7.
[65] S.P. Burke, T.E.W. Schumann, Diffusion flames, Ind. Eng. Chem. 20 (1928) 998–1005. doi:10.1021/ie50226a005.
[66] K.H. Sohn, Z. Rusak, A.K. Kapila, Effect of near-critical swirl on the Burke-Schumann reaction sheet, J. Eng. Math. 54 (2006) 181–196. doi:10.1007/s10665-005-9014-1.
[67] M. Escudier, Vortex breakdown: Observations and explanations, Prog. Aerosp. Sci. 25 (1988) 189–229. doi:10.1016/0376-0421(88)90007-3.
[68] S. Uchida, Y. Nakamura, M. Ohsawa, Experiments on the Axisymmetric Vortex Breakdown in a Swirling Air Flow, Japan Soc. Aeronaut. Sp. Sci. Trans. 27 (1985) 206–216. http://adsabs.harvard.edu/abs/1985JSAST..27..206U.
[69] A. Einstein, Die Ursache der Maanderbildung der FluBlaufe und des sogenannten Baerschen Gesetzes, Naturwissenschaften. 14 (1926) 223–224. doi:10.1007/BF01510300.
[70] C.S. Yogananda, A. Einstein, The cause of the formation of meanders in the courses of rivers and of the so-called Baer's law, Resonance. 5 (2000) 105–108. doi:10.1007/BF02839006.
[71] J. Du, R.L. Axelbaum, The effect of flame structure on soot-particle inception in diffusion flames, Combust. Flame. 100 (1995) 367–375. doi:10.1016/0010-2180(94)00136-G.